Shear stress relaxation and diffusion in simple liquids by molecular dynamics simulations: analytic expressions and paths to viscosity

D.M. Heyes,* E.R. Smith[b],‡ and D. Dini§

Department of Mechanical Engineering,

Imperial College London,

Exhibition Road, South Kensington,

London SW7 2AZ, United Kingdom.

(Dated: April 11, 2019)

[b] and : Department of Mechanical and Aerospace Engineering,

Brunel University London, Uxbridge, Middlesex UB8 3PH, United Kingdom.

Abstract

The results are reported of an equilibrium Molecular Dynamics (MD) simulation study of the shear viscosity, η, and self-diffusion coefficient, D, of the Lennard-Jones liquid using the Green-Kubo (GK) method. Semi-empirical analytic expressions for both GK time correlation functions were fitted to the simulation data and used to derive analytic expressions for the time dependent diffusion coefficient and shear viscosity, and also the correlation function frequency transforms. In the case of the shear viscosity for a state point near the triple point a sech function was found to fit the correlation function significantly better than a gaussian in the ballistic short time regime. A reformulation of the shear GK formula in terms of a time series of time integrals ('viscuits') and contributions to the viscosity from components based on the initial stress ('visclets') enable the GK expressions to be recast in terms of probability distributions which could be used in coarse grained stochastic models of nanoscale flow. The visclet treatment shows that stress relaxation is statistically independent of the initial stress for equilibrium and metastable liquids, suggesting that shear stress relaxation in liquids is diffusion controlled. In contrast, the velocity autocorrelation function is sensitive to the initial velocity. Weak oscillations and a plateau at intermediate times originate to a greater extent from the high velocity tail of the Maxwell-Boltzmann velocity distribution. Simple approximate analytic expressions for the mean square displacement and self van Hove correlation function are also derived.

I. INTRODUCTION

The shear viscosity, η, and self-diffusion coefficient, D, of liquids have been much studied over recent decades by experiment, statistical mechanical theory and Molecular Dynamics (MD) computer simulation. The Green-Kubo (GK) relationships in which the transport coefficient is proportional to the integral of the appropriate time autocorrelation function have played an important role in these investigations.[1] There is a well known strong link between the diffusion coefficient and shear viscosity, for example, as expressed in the Stokes-Einstein relationship,[2,3] and there have been many theoretical studies seeking to understand and quantify the factors determining η and D, and the common factors between them (see *e.g.*, Refs.[2,4]).

In this work accurate semiempirical analytic formulas for the shear stress autocorrelation (SACF) and velocity autocorrelation function (VACF) have been fitted to MD simulation data for a Lennard-Jones (LJ) reference state point near the triple point. These were used to derive analytic expressions for the time dependent viscosity and mean square particle displacement, and the real and imaginary components of the frequency dependent viscosity and self-diffusion coefficient. In the past the focus has been on parametrizing the more basic quantity, the memory function (MF),[5] which was then only able to give approximate representations of the exact (MD) SACF and VACF. The present approach, by fitting the autocorrelation function itself, leads to more practically useful outcomes.

Another aspect of this work is to recast the GK formulas in terms of probability distribution functions. These provide new insights and ways of portraying the decorrelation of property values with time, which is in a form that could be used in building simple stochastic models in the tradition of the Eyring model,[6] and in rejection-based stochastic treatments of nanoscale

flows.

In Sect. II the shear viscosity and related quantities are considered. In Sect. III the self-diffusion coefficient and associated functions are discussed, and conclusions and an overall summary of the work are given in Sec. IV.

II. SHEAR VISCOSITY

The Newtonian shear viscosity, η, is calculated using the GK method by

$$C_s(t) =< \sigma(0)\sigma(t) >, \qquad \eta(t) = \frac{V}{k_B T}\int_0^t C_s(x)dx, \qquad \eta = \lim_{t\to\infty}\eta(t), \tag{1}$$

where $C_s(t)$ is the shear stress autocorrelation function (SACF). The shear stress is minus one of the off-diagonal components of the pressure tensor, *e.g.*, $\sigma_{xy} = -P_{xy}$, which for notational conciseness is referred to here by, σ. The angular brackets indicate an average over different starting times or time origins, defined as $t = 0$. The $C_s(t)$ decays monotonically with time to zero. The so-called time dependent shear viscosity, $\eta(t)$, is defined in the middle expression of Eq. (1), where V is the volume of the simulation cell, k_B is Boltzmann's constant and T is the temperature. The viscosity is the long time limit of $\eta(t)$ as defined in Eq. (1). In practice, this integral is carried out numerically to a time that is sufficiently long for the $C_s(t)$ to be statistically zero but before the statistical noise dominates. One procedure is to average the time integral of $C_s(t)$ over a time period between, $t-\tau$ and t, where τ might be, say, a quarter of the value of the maximum value of t, as follows

$$\eta \simeq \frac{1}{\tau}\int_{t-\tau}^{t}\eta(x)dx. \tag{2}$$

It is important to choose the value of τ such that the correlation function has levelled off by $t - \tau$. Mitigating the generally poor statistical convergence of $C_s(t)$ (as it is calculated from a whole system property) and hence $\eta(t)$ by data smoothing or filtering both with respect to time,[7–9] and system size.[3,10] has been the subject of a number of publications.[11] The response in stress from an infinitesimal step in strain (normalized by the strain step) applied to an equilibrium fluid is called the stress relaxation function in rheology, which is $(V/k_BT)C_s(t)$ in the present notation.

Another approach is to fit an analytic function to the simulation $C_s(t)$ or stress relaxation function data and then integrate this analytically to determine the viscosity. This might be viewed as being just an alternative way of improving the statistics of the viscosity, without practical advantage over Eq. (2). However, it also provides additional benefits, in that it gives directly analytic expressions for $\eta(t)$ and the frequency dependent complex viscosity, $\eta(\omega)$, which can be used in other theoretical and practical modelling applications. Also the terms of the expression could in principle be associated with specific diffusional and stress relaxation mechanisms established by other means, which requires further investigation The procedure of fitting the MD generated SACF to an analytic function is described in the next section.

A. Analytic expression for the stress relaxation function and derived quantities

A number of analytic forms for the stress decay function, $C_s(t)$, have been proposed in the literature.[12] Strictly speaking the time correlation function should be even in time so its time expansion should be in powers of t^2.[1] This is felt predominantly at short time, in the 'ballistic' or early part of the shear stress decay. That is why this part of the time decay has been

This manuscript was accepted by J. Chem. Phys. Click here to see the version of record.

represented by a gaussian or a related function which is an even function in time. Hartkamp *et al.* proposed and explored with MD the following functional form for $C_s(t)$,[12]

$$\begin{aligned} C_s(t) &= G_\infty \left(A\ \exp(-t^2/2\tau_1^2) + B\ \exp(-t/\tau_2) + (1-A-B)\exp(-t/\tau_3) \right), \\ \eta(t) &= \frac{V}{k_B T}\int_0^t C_s(s)ds = G_\infty\ \left(A\tau_1\ \sqrt{\pi/2}\ \mathrm{erf}(t/\sqrt{2}\tau_1)) + B\ \tau_2[1-\exp(-t/\tau_2)] \right) \\ &\quad + G_\infty(1-A-B)\tau_3[1-\exp(-t/\tau_3)], \end{aligned} \tag{3}$$

where G_∞ is the infinite frequency shear rigidity modulus. The dimensionless coefficients, A and B, and the three relaxation times, τ_1, τ_2 and τ_3 can be obtained by least squares fitting the MD-determined $C_s(t)$ to the first formula in Eq. (3). The two exponentials in Eq. (3) are found to reproduce well the long time behavior of $C_s(t)$ beyond the ballistic region. An alternative analytic form to the gaussian where the first term is also even in time, employs the *sech* function,

$$\begin{aligned} C_s(t) &= G_\infty \left(A\ \mathrm{sech(t}/\tau_1) + \mathrm{B}\ \exp(-\mathrm{t}/\tau_2) + (1-\mathrm{A}-\mathrm{B})\exp(-\mathrm{t}/\tau_3) \right), \\ \eta(t) &= G_\infty \left(A\tau_1\ \tan^{-1}[\sinh(\mathrm{t}/\tau_1)] + \mathrm{B}\ \tau_2[1-\exp(-\mathrm{t}/\tau_2)] \right) \\ &\quad + G_\infty(1-A-B)\tau_3[1-\exp(-t/\tau_3)]. \end{aligned} \tag{4}$$

The usefulness of the *sech* function for $C_s(t)$ was also noted in Ref.[13] for the case of the steeply repulsive inverse-power fluid. It has also been used as the memory function in numerous Mori series treatments of transport coefficients.[14–16] The advantage of Eq. (4) over (3) is that the first term tends to an exponential at long times, just as the last two terms. This provides further scope for fitting accurately with a sum of exponentials the MD-generated SACF in the transition period between ballistic to diffusive behavior and further out in time. Note that if $A = 1$ and $B = 0$ the Maxwell relaxation time of the analytic $C_s(t)$ would be, $\tau_M \equiv \eta/G_\infty = \sqrt{\pi/2}\ \tau_1$ and $\pi\tau_1/2$, for the gaussian and sech first terms, respectively, appearing on the right hand sides of Eqs. (3) and (4) for $C_s(t)$. The A, B and relaxation times obtained by fitting are different

This manuscript was accepted by J. Chem. Phys. Click here to see the version of record.

for the gaussian and sech equations.

The frequency dependent viscosity is widely encountered in various models for the dynamics of the liquid on the molecular scale.[17] The real and imaginary parts of the complex viscosity are respectively,[18]

$$\eta'(\omega) = \int_0^\infty C_s(t)\cos(\omega s)ds, \quad \eta''(\omega) = \int_0^\infty C_s(t)\sin(\omega s)ds, \tag{5}$$

where ω is the angular velocity. The two functional forms for SACF given in Eqs. (3) and (4) substituted in Eq. (5) yield,

$$\eta'(\omega) = G_\infty\left(A\tau_1\sqrt{\frac{\pi}{2}}\exp(-\frac{(\omega\tau_1)^2}{2}) + \frac{B\ \tau_2}{1+(\omega\tau_2)^2} + \frac{(1-A-B)\tau_3}{1+(\omega\tau_3)^2}\right), \tag{6}$$

and

$$\eta'(\omega) = G_\infty\left(A\ \tau_1\frac{\pi}{2}\ \mathrm{sech}(\frac{\pi}{2}\omega\tau_1) + \frac{\mathrm{B}\ \tau_2}{1+(\omega\tau_2)^2} + \frac{(1-\mathrm{A}-\mathrm{B})\tau_3}{1+(\omega\tau_3)^2}\right), \tag{7}$$

for the real part of the gaussian and sech formulas, respectively. The imaginary parts of these two analytic forms for the stress relaxation function are,

$$\eta''(\omega) = G_\infty\left(A\tau_1\sqrt{\frac{\pi}{2}}\exp(-\frac{(\omega\tau_1)^2}{2})\ \mathrm{erf}(\omega\tau_1/\sqrt{2}) + \frac{\mathrm{B}\ \omega\tau_2^2}{1+(\omega\tau_2)^2} + \frac{(1-\mathrm{A}-\mathrm{B})\omega\tau_3^2}{1+(\omega\tau_3)^2}\right), \tag{8}$$

for the gaussian of Eq. (3), where erf(x) is the error function of x. For the sech function,[19]

$$\begin{aligned}\eta''(\omega) &= G_\infty\left(-A\frac{\tau_1}{2}[\pi\tanh(\frac{\pi\omega\tau_1}{2}) + i[\psi\left(\frac{1}{4}+i\frac{\omega\tau_1}{4}\right) - \psi\left(\frac{1}{4}-i\frac{\omega\tau_1}{4}\right)] + \frac{B\ \omega\tau_2^2}{1+(\omega\tau_2)^2} + \frac{(1-A-B)\omega\tau_3^2}{1+(\omega\tau_3)^2}\right),\\ &= G_\infty\left(-A\frac{\tau_1}{2}[\pi\tanh(\frac{\pi\omega\tau_1}{2}) - F(\frac{1}{4},\frac{\omega\tau_1}{4})] + \frac{B\ \omega\tau_2^2}{1+(\omega\tau_2)^2} + \frac{(1-A-B)\omega\tau_3^2}{1+(\omega\tau_3)^2}\right),\end{aligned} \tag{9}$$

where ψ is Euler's psi function. The last line of Eq. (9) is a further simplification using the summation, $F(x,y) = \sum_{k=0}^{\infty} 2y/[y^2+(x+k)^2]$ (see Ref.[20], p. 944, Eq. (8.363.4)) which enables routine computation within a standard programing environment.

This manuscript was accepted by J. Chem. Phys. Click here to see the version of record.

The frequency dependent viscosity formulas could be used to include viscoelastic effects in continuum models, by summing over as many frequencies as needed to generate a fluctuating viscosity term.[21] An alternative method of including viscoelastic effects in terms of time rather than frequency is presented in the next section by using the time dependent decorrelation of the shear stress.

The LJ state point, $\rho = 0.8442$ and $T = 0.722$, which is close to the triple point and has become a standard or reference state point for the LJ system,[22] was used to calculate the SACF and viscosity by its numerical integration. The quantities quoted in this work are expressed in the usual LJ pair potential units of energy and distance, and the mass, m, of the molecule. The simulations used to calculate the analytically fitted VACF and SACF data were for $N = 2048$ molecules, with an interaction truncation distance of 2.8, with a tapering of the potential to zero between $r = 2.5$ and 2.8. Computation of the properties shown was for 12×10^6 time steps of magnitude 0.006. Prior to this, equilibration was for 5×10^5 time steps. Time origins for the correlation functions were taken every time step. The uncertainies in the viscosity were less than 2%. The real and imaginary frequency Fourier transforms for the shear stress autocorrelation function had statistical uncertainties of *ca.* $\sim$ 3% and 5%, respectively, and about half these values for the Fourier transform of the velocity autocorrelation function. The simulation codes were written by the authors in FORTRAN 90.

As the shear stress is the sum of a kinetic term (k) and a configurational term (c), there are three components to the shear stress autocorrelation function and hence the shear viscosity (namely, kinetic, kk, cross kinetic-configurational, kc, and configurational, cc).[1] At this density the cc term dominates (see also Table I). The shear viscosity of this state point has been computed many times by different authors, and an average value of them is given in Refs.[23,24].

Table I shows that the viscosity given by the present work *i.e.*, 3.25(3) particles is in statistical agreement with this average of the literature values.

Figure 1(a) presents the $C_s(t)$ obtained by MD and its least squares fit using the gaussian and sech functions defined in Eq. (3) and (4), respectively. The differences between these two fits and the MD data are also shown. The agreement is very good at all times for the sech function, within the simulation statistics. The gaussian expression does not reproduce the MD data as well in the transition region of $\sim 0.15 < t < 0.20$ between the rapidly decaying (ballistic) and slowly decaying (exponential) regions. The contributions to $C_s(t)$ from the three component functions of the fit are also shown in Fig. 1(a). Figure 1(b) shows $\eta(t)$ obtained directly from the MD data and using the analytic functions in Eq. (3) and (4). Just as for $C_s(t)$, best agreement with the MD correlation function is made with the sech containing analytic expression.

Figure 2 shows the corresponding $\eta'(\omega)$ and $\eta''(\omega)$ obtained numerically from the MD stress correlation function (represented by symbols), and from the analytic expressions given in Eqs. (6) to (9), respectively. Numerical Fourier transform integration of the original MD data produces noisy curves. The real part of the transform, $\eta'(\omega)$, decreases monotonically with frequency, and $\eta''(\omega)$ increases from zero and has a peak before descending at higher frequency. Again it can be seen that the sech containing functions agree significantly better with the numerical data than the gaussian cases. The imaginary components are more difficult to obtain accurately at high frequency by applying the sine Fourier transform to the tabulated MD $C_s(t)$.

The viscosities obtained by shearing the liquid using the SLLOD Non-equilibrium Molecular dynamics (NEMD) method,[25,26] are also shown in Fig. 2. For comparison purposes, on the figure, ω, is replaced by $2\pi\dot{\gamma}$, where $\dot{\gamma}$ is the shear rate (the data points are taken from Ref.[6]).

This manuscript was accepted by J. Chem. Phys. Click here to see the version of record.

The shear thinning curve descends more slowly than $\eta'(\omega)$, showing an increasing departure from the Cox-Merz rule,[27] which is a hypothesis based on empirical observation for polymer solutions that for small 'ω' the two quantities are approximately the same. This equivalence is not well obeyed for the LJ liquids.

The viscosity, η, is obtained from the $t \to \infty$ limit of $\eta(t)$ and the $\omega \to 0$ limit of $\eta'(\omega)$. For the gaussian and sech-based $\eta(t)$ functions in Eqs. (3) and (4), for the corresponding $\eta'(\omega)$ given in Eq. (7), these two limits for the Newtonian viscosity are,

$$\begin{aligned} \eta &= G_\infty \left(A\tau_1 \sqrt{\frac{\pi}{2}} + B\tau_2 \ + (1-A-B)\tau_3 \right) \quad \text{gaussian} \\ \eta &= G_\infty \left(A\tau_1 \frac{\pi}{2} + B\tau_2 \ + (1-A-B)\tau_3 \right) \quad \text{sech} \quad . \end{aligned} \tag{10}$$

A classical hydrodynamic treatment predicts that time correlation functions for fluid transport coefficients should decay algebraically at long time,[28] a feature which is not included in the present formulation. At liquid densities other stress relaxation mechanisms derived from structural constraints (*e.g.*, the 'molasses tail',[29]) are also present. Nevertheless, there is still evidence for this algebraic dependence within the simulation statistics at liquid densities.[30–33] Its presence has a dominating effect on the low frequency, $\omega < 1$, behavior of the complex viscosity, and the real part should feature a $\omega^{1/2}$ cusp in this limit.[34]

In the next section an alternative perspective and resolution of the nature of shear stress relaxation mechanism in liquids based on probability distribution functions is reported.

This manuscript was accepted by J. Chem. Phys. Click here to see the version of record.

B. Probability distribution function formulation of the shear viscosity

Assuming that the probability distribution of the shear stress, σ, is gaussian at all times, following the central limit theorem,

$$P(\sigma) = \frac{1}{(2\pi(S(\sigma))^2)^{1/2}} \exp(-\frac{\sigma^2}{2(S(\sigma))^2}), \qquad <\sigma^2> = \int_{-\infty}^{\infty} \sigma^2 P(\sigma) d\sigma = (S(\sigma))^2. \tag{11}$$

where $S(x)$ is the standard deviation of x (noting that the mean shear stress is zero at equilibrium, the limit considered in this work). The Green-Kubo relationship for the shear viscosity can be simplified as follows,

$$\begin{aligned} \eta &= \frac{V}{k_B T} \int_0^{\infty} <\sigma(0)\sigma(t)> dt, \\ &= \frac{V}{k_B T} <\sigma(0)^2> \int_0^{\infty} \frac{<\sigma(0)\sigma(t)>}{<\sigma(0)^2>} dt, \\ &= \frac{V}{k_B T} <\sigma(0)^2> \tau_s, \quad = G_{\infty} \tau_s, \end{aligned} \tag{12}$$

where τ_s is the shear stress relaxation time and G_{∞} is the infinite frequency shear rigidity modulus. Equation (12) shows that Maxwell's identity for the shear viscosity,[35] $\eta = G_{\infty}\tau_s$, emerges naturally from this treatment. As $<\sigma(0)^2> = <\sigma^2>$ the infinite frequency shear modulus is defined by, $G_{\infty} = [V/k_B T] <\sigma^2>$.

2D PDF profiles and the Viscuit

Using the shorthand, $\sigma_0 \equiv \sigma(0)$ and $\sigma_t \equiv \sigma(t)$, a probabilistic representation of the evolution of the shear stress of the whole system is proposed in this section. The relationship between an initial stress value for the whole system, σ_0, and its value, σ_t, at a later time, t, can be expressed in the form of a 2D probability distribution function, an example of which is shown in Fig. 3. This measures in a novel way the decay in correlation between initial and final stresses, which in GK is represented simply by a one dimensional time autocorrelation function. The shear stress at each time in a correlation period t is plotted in a 2D histogram against initial starting

This manuscript was accepted by J. Chem. Phys. Click here to see the version of record.

stress and fitted to a double gaussian expression with a cross-correlation term,[36] of the form,

$$P(\sigma_0, \sigma_t) = \frac{1}{2\pi S(\sigma_0) S(\sigma_t)\sqrt{1-c(t)^2}} \exp\left(\frac{-\left[u_0^2 - 2c(t)u_0u_t + u_t^2\right]}{2(1-c(t)^2)}\right) \tag{13}$$

where $u_\alpha \equiv (\sigma_\alpha - \langle\sigma_\alpha\rangle)/S(\sigma_\alpha)$ for $\alpha = 0$ or $\alpha = t$, and $-1 < c(t) < 1$ is the time dependent correlation coefficient. The stress at the two times is initially completely correlated at $t = 0$, which is represented by a straight line profile at 45^0 (not shown). Figure 3 shows that the profile contours gradually broaden and reorient with time. At very short time, $t = 0.02$, there is still a high correlation coefficient, c, between the two stresses. The decreasing slant angle of the PDF seen in frames, b) and c) for times, 0.05 and 0.1, respectively indicates that the two stresses become less correlated with time. The contours tend to concentric circles, a limit which indicates that the final stress has become completely decorrelated from the initial value. Then the 2D PDF is symmetrical and just the product of two independent gaussian distributions ($i.e.$, $c = 0$). The time dependent correlation coefficient, $c(t)$, is found to be statistically indistinguishable from the normalized autocorrelation, $C_s(t)$, as shown in Fig. 1(a). The significance of this result is that the independently computed $C_s(t)$ or its fitted form given in Eq. (4) can be used in conjunction with the PDF formula in Eq. (13) to represent the stress evolution of the system with time in a probabilistic formulation. If the shear stress at time zero is known, the stress at any later time can be obtained using,

$$\sigma_t = c(t)\sigma_0 + \xi\sqrt{1-c(t)^2} \tag{14}$$

where $c(t)$ ($\equiv C_s(t)$ normalized), is the correlation obtained from Eq. (4), and ξ is a gaussian random number generated using the Box-Muller method,[37] with mean, $< \sigma_t >$, and standard deviation, $S(\sigma_t)$. This provides a method to include the stress correlation history in a higher level Langevin or fluctuating hydrodynamics model.

This manuscript was accepted by J. Chem. Phys. Click here to see the version of record.

The contribution of the sequence of stresses in order of generation to the shear viscosity can be determined by reversing the usual order of the time integral and the ensemble average of the time correlation function in the Green-Kubo formula,

$$\begin{aligned}\eta(t) &= \frac{V}{k_B T}\int_0^t \langle \sigma(0)\sigma(x)\rangle \, dx \\ &= \frac{V}{k_B T}\frac{1}{\tau_r}\int_0^{\tau_r - t} d\tau \int_0^t \sigma(\tau)\sigma(\tau + x) \, dx \\ &= \frac{1}{\tau_r}\int_0^{\tau_r - t} d\tau \int_0^t \eta_u(\tau, x) \, dx \\ &= \langle \eta_u(t)\rangle \quad \text{shorthand} \\ \eta &= \lim_{t\to\infty} \langle \eta_u(t)\rangle \end{aligned} \tag{15}$$

where τ_r is the duration of the sampling (*i.e.*, simulation time). Equation (15) involves a sequence of integrals of a *single* trajectory from (simulation) time, τ to time $\tau + t$ which is written as, $\eta_u(\tau, t)$, which is referred to here as the 'viscuit'. The τ argument is dropped henceforth, as the average over the simulation of many time origins is implicit. This 'hybrid' reformulation of GK (in a time origin averaged sense) is not new and was discussed by Erpenbeck,[28] but its properties were not explored in that work, and not in the context of single trajectories. A similar hybrid reformulation of the Green-Kubo formula was investigated for self-diffusion in Ref.[38].

The viscosity is obtained from the average of the infinite time limits of the $\eta_u(t)$. Note that a viscuit can be negative unlike the viscosity itself. Figure 4(a) shows the probability density function of viscuits, $P(\eta_u)$ which is like a Laplace distribution but is in fact skewed to the right, as the total viscosity, the 1st moment of this probability distribution,

$$\begin{aligned}\eta &= \int_{-\infty}^{\infty} \eta_u P(\eta_u) d\eta_u \\ &= \int_0^{\infty} \eta_u [P(\eta_u) - P(-\eta_u)] d\eta_u \end{aligned} \tag{16}$$

must be non-zero and positive. The blue line is the MD viscuit PDF, which is peaky and skewed to the right due to the correlation between the time dependent sequence of stress values

This manuscript was accepted by J. Chem. Phys. Click here to see the version of record.

during system's correlation time. The red curve is the distribution from an autocorrelation of two independent gaussian random number distributions. The dashed black curve was generated from correlated gaussian numbers using Eqs. (4) and (14). The red curve is not skewed whereas the black curve is skewed. The correlated gaussian model exaggerates the extent of skewness compared with the direct MD viscuit results because the correlating function, $c(t)$, is never negative (as it is a system average property). The random numbers can give negative values, and that is why the distribution extends into the negative quadrant. The purely MD generated case (blue curve) has a standard deviation which is about seven times larger than the other two, which may be attributed to the wide tails on both sides in that case. The MD distribution is skewed to the positive side because the initial values of stress are strongly correlated, and therefore large positive viscuits are more likely than negative ones. The shape of the distribution is not gaussian, indicating that the mean is not the most representative of the range of possible autocorrelations in each of the systems. Negative viscuits are highly probable, almost as likely as positive ones, and as a result the viscosity of the system computed from this distribution is the difference between two large numbers.

Figure 4(b) presents on the abscissa the logarithm of the ratio, R, of positive to negative viscuits with the same $|\eta_u|$, obtained from the PDF in Fig. 4(a), which indicates that,

$$R = \frac{P(\eta_u > 0)|\eta_u)}{P(\eta_u < 0)|\eta_u)} = e^{A|\eta_u|}, \tag{17}$$

where the constant, A, decreases with time. Equation (17) bears some similarity with the Fluctuation Theorem (FT) and its relationship to Green-Kubo.[39–42] Although in the FT the time averaged shear stress due to a finite shear rate is the independent variable, here it is the viscuit, which is the integral of the product of two shear stresses at different times. Simply including correlated random noise is not sufficient to capture the full underlying complexity of the MD

This manuscript was accepted by J. Chem. Phys. Click here to see the version of record.

model, as is demonstrated in Fig. 4(b) which shows the viscuit PDF generated assuming the correlated gaussian model of Eq. (13) (the dashed curve). This has a much smaller standard deviation and a very different shape.

Figure 5(a) shows a plot of $A(t)$ defined in Eq. (17) and derived from the MD data for a range of integration intervals, t. The figure also shows a fit to these data using the functional form, $A(t) = A_1 + A_2/t^{A_3}$, which matches well for not too small t. $A(t)$ must tend to a non-zero limit in the large time limit for $P(\eta_u)$ to be asymmetric and therefore the viscosity to be nonzero and positive using the definition of the viscosity given in Eq. (16).

A 2D map of initial stress against the resulting viscuit is given in Fig. 5(b) (Multimedia view). This plot was generated by first starting at time step 1 with stress σ_1 from which the values of the first viscuit were plotted with time. Then the viscuit starting from time step 2 with stress σ_2 was plotted after that. The sequence of points gives a chaotic distribution of points. It reveals that the initial stress and viscuit are correlated for a period of time. Some trajectories switch over a small number of time steps to being anti-correlated (*i.e.*, a negative viscuit). There are intermittent jumps of the map path from one part of the diagram to another in Fig. 5(b) (Multimedia view), which could be a reflection of the system moving from one inherent structure or metabasin to another.[43,44] The final butterfly shape of the map indicated by the contour lines on Fig. 5(b) is a consequence of the definition of viscuit and a reflection of the underlying dynamical processes. Small initial stresses typically result in small viscuits, and in the limit, an initial stress of zero means that the viscuit can only be zero at all times. Vertical slices taken through the distribution at arbitrary values of initial stress, σ_0, give a gaussian density distribution of viscuits which becomes narrower with decreasing (absolute) initial stress. A high initial stress typically results in a larger viscuit ('viscosity') and a non-symmetrical distribution

This manuscript was accepted by J. Chem. Phys. Click here to see the version of record.

about the ordinate axis reflects the effect of positive correlations on average at all times. From Eq. (16) there have to be more points above the ordinate axis than below for the total viscosity to be positive. The corresponding plot for the random correlated noise case (corresponding to the black dashed line in Fig. 4(a)) shows a large positive viscuit lobe and a small negative lobe.

The single trajectory 'viscosity' or viscuit provides useful information about the shear stress evolution in the system which would complement quasi-harmonic models of the liquid state,[45,46] as it characterizes the time evolution of the stress on the potential energy landscape. In the next section another type of PDF resolution of the stress evolution is introduced.

Green-Kubo initial stress resolution and the Visclet

The GK expression can be written in PDF form as a function of the initial stress, σ_0. Let $P(\sigma_0)$ be the probability distribution of σ_0, then the shear viscosity can be written,

$$\begin{aligned}
\eta &= \frac{V}{k_B T}\int_{-\infty}^{\infty} P(\sigma_0) \int_0^{\infty} <\sigma_0\sigma_t> dt\ d\sigma_0, \\
&= \frac{V}{k_B T}\int_{-\infty}^{\infty} \sigma_0^2 P(\sigma_0) \int_0^{\infty} \frac{<\sigma_0\sigma_t>}{\sigma_0^2} dt\ d\sigma_0, \\
&= \frac{V}{k_B T}\int_{-\infty}^{\infty} \sigma_0^2 P(\sigma_0) \int_0^{\infty} C_{s,0}(t) dt\ d\sigma_0, \\
&= \frac{V}{k_B T}\int_{-\infty}^{\infty} \sigma_0^2 P(\sigma_0)\ \tau_{s,0}\ d\sigma_0, \\
&= \frac{G_\infty}{<\sigma^2>}\int_{-\infty}^{\infty} \sigma_0^2 P(\sigma_0)\ \tau_{s,0}\ d\sigma_0, \\
&= G_\infty \frac{\int_{-\infty}^{\infty} \sigma_0^2 P(\sigma_0)\ \tau_{s,0}\ d\sigma_0}{\int_{-\infty}^{\infty} \sigma_0^2 P(\sigma_0)\ d\sigma_0}, \\
&= G_\infty \int_{-\infty}^{\infty} E(\sigma_0)\ \tau_{s,0}\ d\sigma_0, \\
&= \int_{-\infty}^{\infty} E(\sigma_0)\eta_{s,0}\ d\sigma_0, \\
&= G_\infty \tau_s
\end{aligned} \tag{18}$$

where the definition of G_∞ from Eq. (12) has been used. The relaxation time, $\tau_{s,0}$, is that

This manuscript was accepted by J. Chem. Phys. Click here to see the version of record.

associated with a starting stress, σ_0, and

$$C_{s,0}(t) = \frac{<\sigma_0\sigma_t>}{<\sigma_0^2>}, \quad \tau_{s,0} = \int_0^\infty C_{s,0}(t)dt, \quad E(\sigma_0) = \frac{\sigma_0^2 P(\sigma_0)}{\int_{-\infty}^{\infty}\sigma_0^2 P(\sigma_0)d\sigma_0}, \quad \eta_{s,0} = G_\infty\,\tau_{s,0}. \quad (19)$$

The quantity, $\eta_{s,0}$, is henceforth called the 'visclet', which after time averaging is the contribution to the total viscosity from those initial states which at $t = 0$ have a particular value of the stress, σ_0. The viscuit and visclet are formally related through, $\eta_{s,0} =< \eta_u(t,\sigma_0) >_0$ *i.e.*, the visclet is the ensemble average of the viscuits for which the starting stress is σ_0. The corresponding relaxation time of these states is $\tau_{s,0}$. The function, $E(\cdots)$, is the weight given to the $G_\infty\tau_{s,0}$ contribution to the viscosity. Therefore the Green-Kubo formula is now expressed in terms the σ_0-component correlation functions and relaxation times. If $\tau_{s,0}$ is independent of σ_0 then the system is described by only one relaxation time and Eq. (12) is recovered, otherwise the more general expression given in Eq. (18) is required.

To implement this initial stress resolution numerically in a computation, the visclets are collected in a histogram of limited ranges of σ_0. A set of $M+1$ stresses, $\sigma_1 < \sigma_2 < \sigma_3 \cdots < \sigma_{M+1}$ specify the boundaries of the M (≤ 120) elements of $C_s(t,\sigma_0) \equiv C_{s,0}(t)$ defined in in Eq. (19). Each bin index i corresponds to a limited range of σ_0,

$$C_{s,i}(t) = G_\infty \int_0^\infty [H(\sigma_{i+1} - \sigma_0) - H(\sigma_i - \sigma_0)]\frac{<\sigma_0\sigma_t>}{<\sigma_0^2>}d\sigma_0, \quad (20)$$

where $H(\cdots)$ is the Heaviside step function.

Figure 6(a) shows the probability distribution function, $P(\sigma_0)$, and the PDFs of the $\eta_{s,0}$ and $\tau_{s,0}$ as a function of the initial stress in dimensionless form as, $\sigma_0/S(\sigma_0)$. The figure confirms that the stress PDF is gaussian (the least squares fit is shown). Also the $\eta_{s,0}$ PDF is essentially, $\sigma_0^2 P(\sigma_0)$, as $\tau_{s,0}$ only very weakly depends on σ_0. Figure 6(b) presents the same data plotted

on a lin-log scale, to reveal the wide range of stresses for which the gaussian approximation is valid. Figure 6 reveals that the relaxation times are only very weakly dependent on the initial shear stress.

Figure 7 shows the total SACF for three LJ state points, the standard one used above, and two metastable fluid states. One of the metastable states is along the zero pressure isobar and is above the glass transition, which is at *ca.* $T = 0.29$ and $\rho = 0.98$.[47,48] A supercooled liquid shows dynamical heterogeneities,[49] which one might expect would have an effect on the SACF. The total SACF (shown in green) decays slower at long times as the system goes further into the metastable region, and in each case as an exponential. Ladd *et al.*,[29] showed that at high density structural orientational time evolution correlates well with the shear-stress autocorrelation function, which decays as a stretched exponential with a density independent exponent. Exponential fits to the three $C_s(t)$ for $t > 0.4$ are also shown on the figure. Figure 7 also presents the normalized $C_{s,0}(t)$ defined in Eq. (19) where the initial stress is taken within four bands of initial stress relative to the standard deviation of the stress, $\sigma_0/S(\sigma_0)$. Components resolved for initial stresses of $\sigma_0/S(\sigma_0)$ in the ranges, $0-1$, $1-2$, $2-3$ and $3-4$ reveal that the curves are statistically indistinguishable, which is consistent with the conclusions from Fig. 6, and suggests that stress decay in dense fluids is determined by the relative diffusion of the molecules rather than by a stress activated process. The nature of self-diffusion in these systems is considered in the next section.

This manuscript was accepted by J. Chem. Phys. Click here to see the version of record.

III. SELF-DIFFUSION

The self-diffusion coefficient can be calculated by either the Einstein-Helfand (EH) equations,

$$\Delta r^2(t) = \frac{1}{N}\sum_{i=1}^{N}\left(\underline{r}_i(t) - \underline{r}_i(0)\right)^2, \qquad D = \lim_{t\to\infty}\frac{\Delta r^2(t)}{6t}, \qquad D = \lim_{t\to\infty}\frac{1}{6}\frac{d\Delta r^2(t)}{dt}, \tag{21}$$

or a Green-Kubo (GK) formula,[1] employing the velocity autocorrelation function (VACF),

$$C_v(t) = <\underline{v}(s)\cdot\underline{v}(0)>, \qquad D'(t) = \frac{\Delta r^2(t)}{6t} = \frac{1}{3}\int_0^t (1-\frac{s}{t}) <\underline{v}(s)\cdot\underline{v}(0)> ds, \tag{22}$$

where $D'(t)$ may be considered to be an effective time dependent diffusion coefficient. The link between Eqs. (21) and (22) is (see Ref.[1] p. 272),

$$\Delta r^2(t) = 2t\int_0^t (1-\frac{s}{t}) <\underline{v}(s)\cdot\underline{v}(0)> ds. \tag{23}$$

The first route to D in Eq. (21) takes the form $D(t) = A/6t + D$ (where A is a constant) for large t, and the $O(t^{-1})$ term is slow to converge with t. The third (time derivative) route to D in Eq. (21) converges more rapidly. Applying Leibniz's rule (see Ref.[50] p. 335) to Eq. (23) then,

$$D(t) = \frac{1}{6}\frac{d\Delta r^2(t)}{dt} = \frac{1}{3}\int_0^t <\underline{v}(s)\cdot\underline{v}(0)> ds, \qquad D = \lim_{t\to\infty} D(t) \tag{24}$$

which is the equation usually found in the literature for D rather than Eq. (22). The same derivation steps lead to the corresponding definition of the time dependent viscosity already given in Eq. (1) (*i.e.*, without the $(1-[s/t])$ factor).

Figure 8(a) presents the normalized VACF obtained for the reference LJ state point by MD. The normalized force autocorrelation function (FACF), $C_F(t) = <\underline{F}(t)\cdot\underline{F}(0)> / <F(0)^2>$ is also given on the figure. For dense fluids the form of the VACF is determined primarily by the interaction of the particle with its first coordination shell.[51] The effect of increasing the attractive forces in addition to a short range repulsion is to enhance the cohesiveness of the

This manuscript was accepted by J. Chem. Phys. Click here to see the version of record.

cages,[52] and to delay crystal nucleation to lower temperatures.[53]

The analytic form of the VACF has been explored in the literature.[54] Previous theoretical descriptions of the VACF and diffusion coefficient have been based on the hard sphere (*i.e.*, Enskog) approximation, or the more indirect memory function approach,[14–16] with an assumed form for the memory function.

A. Analytic expression for the velocity autocorrelation function and derived quantities

The MD simulation generated VACF can be represented to a good approximation by the analytic function,

$$C_v(t)/C_v(0) = \exp(-(t/\tau_1)^2) + At^2\exp(-(t/\tau_2)^2) + Bt^2\exp(-t/\tau_3) + Ct^4\exp(-t/\tau_4). \quad (25)$$

where A, B and C have units of time to the power $-2, -2$ and -4, respectively. The terms in Eq. (25) are inspired by formulas for the memory function proposed about 50 years ago.[55–57] The first two terms in Eq. (25) are composed of gaussians rather than the sech function used for $C_s(t)$ in Eq. (4). Figure 8 compares the MD generated VACF with a least squares fit using the new expression in Eq. (25). The green curve on the figure is the difference between the MD-generated and fitted VACF, which may be seen to be very small at all t even though the VACF has a rather difficult damped oscillatory shape to match.

Figure 8(b) presents $D(t)$ from Eq. (24) taking the $C_v(t)$ directly from the MD simulations and its fit using Eq. (25). From Eq. (25) the time dependent diffusion coefficient, $D(t)$, is

$$D(t) = \frac{1}{3}\int_0^t < \underline{v}(s)\cdot\underline{v}(0) > ds,$$

This manuscript was accepted by J. Chem. Phys. Click here to see the version of record.

$$= \frac{k_BT}{m}[\frac{1}{2}\tau_1\sqrt{\pi}\ \mathrm{erf(t/\tau_1)} + \mathrm{A}\left(-\frac{1}{2}\mathrm{t}\tau_2^2\exp(-(\mathrm{t}/\tau_2)^2) + \frac{\sqrt{\pi}\tau_2^3}{4}\mathrm{erf(t/\tau_2)}\right)$$
$$-B\tau_3^3\left((t/\tau_3)^2 + 2(t/\tau_3) + 2\right)\exp(-t/\tau_3) + 2B\tau_3^3$$
$$-C\tau_4^5\left((t/\tau_4)^4 + 4(t/\tau_4)^3 + 12(t/\tau_4)^2 + \ 24(t/\tau_4) + 24\right)\exp(-t/\tau_4) + 24C\tau_4^5]. \quad (26)$$

Equation (26) for $D(t)$ in the $t \to \infty$ limit gives for the self-diffusion coefficient,

$$D = \frac{k_BT}{m}\left(\frac{\sqrt{\pi}}{2}\tau_1 + \frac{\sqrt{\pi}}{4}A\tau_2^3 + 2B\tau_3^3 + 24C\tau_4^5\right). \quad (27)$$

The mean square displacement itself gives another perspective on the transition from ballistic dynamics at short time to the diffusion regime, and some expressions for this quantity have been proposed previously to represent this change.[58,59] The following expression reproduces the simulation data reasonably well,

$$\Delta r^2(t) = A - B\ \mathrm{sech([t-\delta t]/\tau_d)} + 6\mathrm{D\ t}, \quad (28)$$

where D is the self-diffusion coefficient, and A, B, δt and τ_d are positive constants. The sech term captures the deviation at short time of the MSD from the long time limiting formula, $A+6Dt$. Figure 9 presents $\Delta r^2(t)$ calculated directly from the particle coordinates and from the velocity autocorrelation function using Eq. (23), both by MD. The figure also shows the long time limiting formula, $A+6Dt$, and the difference between this and the actual MSD *i.e.*, the sech term in Eq. (28). The least squares fit parameter values are given in the figure caption. The δt term is introduced because at short times when $\Delta r^2(t) \simeq 3k_BTt^2/m$ the correction to the diffusive limit formula has a maximum.

MD simulations of Alder and Wainwright,[60] revealed that the VACF decays algebraically at long times as, $\sim t^{-3/2}$ in 3D. Other studies,[61–65] support this asymptotic behavior, which leads to a cusp in the frequency dependent diffusion coefficient at the origin.[64] This long time tail has only been observed at intermediate densities, as far as we are aware however.[66] The value

This manuscript was accepted by J. Chem. Phys. Click here to see the version of record.

of t when this limiting behavior dominates is not specified by the theory, and therefore its contribution to D is difficult to assess. At liquid densities coupling between the single particle motion to longitudinal and transverse momentum current density correlation functions,[62,67,68] also become important, as another factor determining the VACF and hence the diffusion coefficient.

The normalized power spectrum (PDF) of the VACF has been frequently investigated and calculated, in part because of its relevance to quasi-harmonic and itinerant oscillator models of molecular motion in liquids.[57,63,69–72] Since Rahman's 1964 pioneering study,[73,74] the form of the VACF power spectrum has been interpreted in terms of a combination of low frequency (diffusive) and high frequency (oscillatory) modes, with an overlap region in the frequency PDF obtained by MD.[75]

The real and imaginary parts of the Fourier Transform of the VACF are,

$$D'(\omega) = \int_0^\infty C_v(t)\cos(\omega s)ds, \quad D''(\omega) = \int_0^\infty C_v(t)\sin(\omega s)ds, \tag{29}$$

respectively. Note that the unnormalized VACF is used. From Eq. (25) substituted in (29),

$$\begin{aligned} D'(\omega) = \frac{k_BT}{m}\sqrt{\frac{\pi}{2}}[\frac{\tau_1}{\sqrt{2}}\exp(-(\omega\tau_1)^2/4) \ + \sqrt{2}\frac{A}{8}\tau_2^3\left(2-(\omega\tau_2)^2\right)\exp(-(\omega\tau_2)^2/4)] \\ +2\frac{k_BT}{m}B\tau_3^3\left(\frac{(1-3(\omega\tau_3)^2)}{(1+(\omega\tau_3)^2)^3}\right) \ + 24\frac{k_BT}{m}C\tau_4^5\left(\frac{(1-10(\omega\tau_4)^2+5(\omega\tau_4)^4)}{(1+(\omega\tau_4)^2)^5}\right) \end{aligned} \tag{30}$$

and

$$\begin{aligned} D''(\omega) = \frac{k_BT}{m}\sqrt{\frac{\pi}{2}}[-i\tau_1\sqrt{\frac{1}{2}}\exp(-(\omega\tau_1)^2/4))\mathrm{erf}(\frac{\mathrm{i}\omega\tau_1}{2}) \ + \mathrm{A}\sqrt{\frac{2}{\pi}}\mathrm{F}(\omega\tau_2,\tau_2)] \\ +2\frac{k_BT}{m}B\tau_3^3\frac{(3(\omega\tau_3)-(\omega\tau_3)^3)}{(1+((\omega\tau_3)^2)^3} \ + 24\frac{k_BT}{m}C\tau_4^5\ \frac{(5(\omega\tau_4)-10(\omega\tau_4)^3+(\omega\tau_4)^5)}{(1+(\omega\tau_4)^2)^5}, \end{aligned} \tag{31}$$

where $i\ \mathrm{erf}(\mathrm{ix}) = -(2/\sqrt{\pi})\sum_0^\infty \mathrm{x}^{2\mathrm{k}+1}/(2\mathrm{k}+1)\mathrm{n}!$, and x is real. Also,

$$F(z,\tau_2) = \frac{\sqrt{\pi}\tau_2^3}{4}\ \sum_{k=0}^{\infty}\frac{(-1)^k z^{2k+1}(1+k)4^{-k}}{\Gamma(\frac{3}{2}+k)}$$

This manuscript was accepted by J. Chem. Phys. Click here to see the version of record.

$$= \frac{\tau_2^3}{4}\left([\omega\tau_2] - i(2-[\omega\tau_2]^2)\frac{\sqrt{\pi}}{2}\exp(-(\omega\tau_2)^2/4)\mathrm{erf}(\frac{\mathrm{i}\omega\tau_2}{2})\right). \quad (32)$$

The contributions to $D'(\omega)$ and $D''(\omega)$ from each term in the fit function for $C_s(t)$ are presented for the near triple point state point in Figs. 10(a) and (b), respectively. The real part of the Fourier transform has a peak at $\omega \simeq 10$, which is lower than the Einstein frequency, ω_0 ($\simeq 17$, see Table I) and tends to D in the $\omega \to 0$ limit. The first gaussian term is monotonically decaying and the other three are oscillatory in Fig. 10(a). The imaginary part of the Fourier transform rises from 0 at $\omega = 0$ and has a weak maximum at $\omega \simeq 25$. The first term in Eq. (25) dominates the total function at high frequency, while the remaining terms are oscillatory.

Figure 11 shows the high frequency limit of $D'(\omega)$ and $D^* = [(D')^2 + (D'')^2]^{1/2}$ which indicates that the power law formula, A_p/ω^p, where $p = 6$, fits the D' data well for *ca.* $\omega > 35$. Also the function, $D' = A_a(\tau_a\omega)^q \exp(-(\tau_a\omega)^q)$, where τ_a, p and q are obtained from the analytic formulas given in Ref.[76] matches the simulation D' quite well in this high frequency range (A_a is treated as a fit parameter).

The probability distribution of the velocity follows the Maxwell-Boltzmann distribution,

$$P(v_x) = \frac{1}{(2\pi k_B T/m)^{1/2}}\exp(-\frac{mv_x^2}{2k_B T}), \quad (33)$$

where the standard deviation of the $x-$component of the velocity, v_x is $\sqrt{k_B T/m}$. The VACF was calculated as a function of the initial speed, with element i of the histogram defined by,

$$C_{v,i}(t) = \int_0^\infty [H(v_{i+1} - |v_{x,0}|) - H(v_i - |v_{x,0}|)]\frac{< \underline{v}_{x,0}\underline{v}_{x,t} >}{< v_{x,0}^2 >} d|v_{x,0}|, \quad (34)$$

for the $x-$component of the velocity. The $C_{v,i}(t)$ is the numerical evaluation of the initial speed resolved VACF or $C_{v,0}(t)$. The $C_{v,i}(t)$ in four bands of speed in units of the standard deviation are shown in Fig. 12. The figure shows that much of the solid-like ('cage related')

This manuscript was accepted by J. Chem. Phys. Click here to see the version of record.

oscillatory behavior evident at intermediate times arises from states where the initial velocity is greater than the root mean square velocity. Molecules with initially high kinetic energy are more likely to invoke a reaction from the cage of surrounding molecules, to give rise to the weak oscillations in the VACF in the approximate time range, $0.4 < t < 0.6$, trends which are consistent with previous simulation studies of the exchange of momentum between a molecule and its neighbors.[77,78]

The self part of the van Hove correlation function, $G_s(r,t)$,[79–81] represents the spread of distances, Δr, a molecule executes in time t (*i.e.*, $r = 0$ at $t = 0$),

$$G_s(r,t) = \left(\frac{3}{2\pi < r^2(t) >}\right)^{3/2} \exp\left(-\frac{3\mathrm{r}^2}{< \mathrm{r}^2(\mathrm{t}) >}\right), \tag{35}$$

where $< r^2(t) >$ can be approximated by the formula in Eq. (28). The function, $W(r,t)$, (see Ref.[1] p. 347),

$$W(r,t) = 4\pi r^2 G_s(r,t) \tag{36}$$

is more conveniently plotted. This is because the progression of $G_s(r,t)$ with increasing time is dominated by its divergent $t \to 0$ limiting values, which are also very noisy as $r \to 0$. Figure 13(a) shows that the $W(r,t)$ for three times computed directly in the MD simulations agrees quite well with the analytic solution given in Eq. (35).

The set of even moments of the particle displacements with time are, $\Delta r_{2k}(t) =< (\underline{r}(t) - \underline{r}(0))^{2k} >$, for $k = 1, 2, 3, \cdots$. The non-gaussian parameter,[57,74,82,83] $\alpha(t) = 3[\Delta r_4(t)/\Delta r_2^2]/5 - 1$ represents the departure of the displacements from a gaussian distribution at short and intermediate times. Figure 13(b) compares $\alpha(t)$ with the mean square displacement. As has been noted in previous studies the spread of particle displacements is non-gaussian for times *much* larger than those at which the MSD starts to exhibit a linear time dependence (*i.e.*, the

'diffusive' regime).[84] Therefore this behavior is not confined to certain types and shapes of molecule but is present even in simple liquids of spherical particles, as has been known for a few decades since the pioneering work of Rahman. At the state point considered even at $t = 10$ the particle on average only diffuses about half a molecular diameter. The $\alpha(t) \neq 0$ behavior is due to the intermittency of the molecule's dynamics in different cage geometries and the long time it takes the molecule to escape from its initial cage into a more spatially homogeneous environment. Nevertheless in these systems, the deviations from a gaussian PDF are rather small, as may be seen in Fig. 13(a), despite the differences in the higher moments indicated by $\alpha(t)$.

This manuscript was accepted by J. Chem. Phys. Click here to see the version of record.

IV. CONCLUSIONS

This work is concerned primarily with the Green-Kubo (GK) method used to compute the shear viscosity, η_s and self-diffusion coefficient, D, by equilibrium Molecular Dynamics simulation. A popular state point near the triple point of the Lennard-Jones liquid was used for most of the simulations, and some calculations were carried out at higher density and lower temperature in the metastable liquid part of the phase diagram. Although this is a field which has been studied extensively since the pioneering work of Rahman in the 1960s,[73,74] a number of new aspects of it are revealed in this work. For the shear viscosity of the near triple point state an accurate analytic expression for the shear stress autocorrelation function was obtained by fitting a semi-empirical expression to the simulation data. A formula based on a sech rather than gaussian function for the short time region was found to reproduce the simulation data better. This function was used to derive analytic expressions for the time dependent viscosity, and real and imaginary parts of the complex viscosity. These accurate analytic representations of the shear stress autocorrelation function can therefore also be used in other theoretical models. The same procedure was carried out for the velocity autocorrelation function and D. In the diffusion case, analytic expressions for the time dependence of the mean square displacement and diffusion coefficient were also obtained, and used to define a completely analytic formula for the self part of the van Hove correlation function.

Time correlation functions give an average smoothly varying representation of the decorrelation of property values with time. In contrast, decorrelation of individual trajectories is far from being predictable, showing wildly chaotic and structure dependent behavior. This is explored in this work by rewriting the usual Green-Kubo shear viscosity formula in two different ways which bring out the stochastic nature of the underlying processes in a probability distribution

function (PDF) description. The first analysis was to reverse the usual order of integrating with time the ensemble averaged shear stress autocorrelation function (SACF), to instead express the viscosity as a time sequence of *single* trajectory time integrals or 'viscuits'. The viscosity is the first moment of the probability distribution of long time viscuits. The time-ordered sequence of viscuits as a function of the initial stress on a 2D projection takes the form of a chaotic 2D trajectory with sudden 'jumps' to different points on a 'butterfly' shaped map. The viscuit probability distribution has a Laplacian-like form but is skewed to positive values, which cannot be reproduced by partly stochastic models as its important features are a consequence of the deterministic evolution of the system. The ratio of positive to negative viscuit PDF values is shown to be an exponential function of the absolute viscuit value. A 2D map of the shear stress against its value at a time later showed a transition from perfect correlation to total decorrelation (a series of concentric circles) at long times. This transition can be represented accurately by a double gaussian expression with a cross-correlation term, a formula which could be used in rejection sampling coarse grained continuum models of flow on the nanoscale.

The second decomposition of GK was to resolve the ensemble averaged time correlation function, $C_s(t)$, into components differentiated by the initial stress. The ensemble averaged time integral of each component of $C_s(t)$ is referred to as a 'visclet'. Perhaps surprisingly the normalized component SACFs were shown to be statistically independent of initial stress, which may suggest that shear stress relaxation in liquids is diffusion rather than stress controlled. The probability distributions of stress were gaussian, and was a stress squared scaled gaussian for the visclets, which is consistent with the cross-section slices of the 2D viscuit map in Fig. 5(b). In contrast, the corresponding decomposition of the velocity autocorrelation function (VACF) was found to be a function of initial velocity. The intermediate time plateau and weak oscillatory feature in the VACF at long times was shown to be determined to a greater extent

by those particles with large initial velocities (above the root mean square value). This is consistent with the picture that these features in the VACF are caused by the response of the cage to the molecule-cage 'collision' (*i.e.*, when the VACF goes from being positive to negative).

The various aspects of this work, when combined, open up the prospect of using time correlation function and Green-Kubo calculations obtained by MD simulation as input to parametrize coarse grained stochastic models of liquid flow on the nanoscale. Such a hybrid model would be on a time and distance scale intermediate between the fully molecular and continuum descriptions.

ACKNOWLEDGMENTS

The authors would like to acknowledge the support received from the EPSRC under the Established Career Fellowship Grant No. EP/N025954/1. All data can be made available by emailing the authors of the paper or tribology@imperial.ac.uk.

quantity		quantity		quantity		literature,[23]
u_r	5.815(1)	D_{msd}	0.0335(3)	η_s^{kk}	0.050(1)	0.051(1)
u_a	−11.898(2)	$< F^2 >$	592(1)	η_s^{kc}	0.075(5)	0.060(1)
u	−6.083(2)	$< F^4 > /10^6$	1.07(1)	η_s^{cc}	3.13(2)	3.15(3)
P_{tot}	0.157(1)	$M_{v,2}$	274(1)	η_s^{tot}	3.25(3)	3.29(3)
Z	0.2575(2)	$M_{v,4}/10^5$	2.33(1)	$r_{min,1}$	1.541(1)	
G_∞^c	23.46(1)	$M_{F,2}$	838(1)	$g(r_{min,1})$	0.576(1)	
G_∞	24.07(1)	$M_{F,4}/10^6$	1.79(1)	$r_{max,2}$	2.071(1)	
$M_{s,2}$	297(1)	$r_{max,1}$	1.086(1)	$g(r_{max,2})$	1.283(1)	
$M_{s,4}/10^6$	−6.66(3)	$g(r_{max,1})$	3.018(1)	ω_0	16.52(1)	

TABLE I. Physical properties of the LJ state point, $\rho = 0.8442$ and $T = 0.722$, from an MD simulation of $N = 6912$ particles, with an interaction truncation distance of 3.5, and for a production simulation time of, $t_{sim} = 9415$. The quantities, u_r and u_a are the repulsive and attractive components of the potential energy per particle, u; P_{tot} is the total pressure; Z is the compressibility factor; G_∞^c is the interaction part of the infinite frequency shear rigidity modulus, G_∞; $M_{X,2}$ and $M_{X,4}$ are the 2nd and fourth frequency moments,[85] of the $X-$property autocorrelation function, where v and F are the velocity and force on a molecule, and s denotes the shear stress; ω_0 is the Einstein frequency,[1]; $< F^2 >$ and $< F^4 >$ are the second and fourth moments of the particle force. $g(r_{max,1})$ is the value of the RDF at its first peak and at $r = r_{max,1}$; $g(r_{min,1})$ is the value of the RDF at its first minimum at $r = r_{min,1}$. The numbers in brackets are the statistical uncertainty in the last digit.

References

* d.heyes@imperial.ac.uk

‡ Edward.Smith@brunel.ac.uk

§ d.dini@imperial.ac.uk

[1] J.-P. Hansen and I.R. McDonald, *Theory of simple liquids*, 4th. ed. (Academic Press, Amsterdam, 2013).

[2] L. Costigliola, D. M. Heyes, T. B. Schrøder and J. C. Dyre, J. Chem. Phys. **150**, 021101 (2019).

[3] V.A. Levashov, J.R. Morris and T. Egami, J. Chem. Phys. **138**, 044507 (2013).

[4] U. Balucani, R. Vallauri, T. Gaskell and M. Gori, J. Phys.: Solid State Matt. **18**, 3133 (1985).

[5] U. Balucani, M.H. Lee and V. Tognetti, Phys. Rep. **373**, 409 (2003).

[6] D.M. Heyes, D. Dini and E.R. Smith, J. Chem. Phys. **148**, 194506 (2018).

[7] B. Hess, J. Chem. Phys. **116**, 209 (2002);

[8] L. de Sousa Oliveira and P.A. Greaney, J. Chem. Phys. **95**, 023308 (2017).

[9] R.E. Jones and K.K. Mandadapu, J. Chem. Phys. **136**, 154102 (2012).

[10] V.A. Levashov, J. Chem. Phys. **141**, 124502 (2014).

[11] Y. Zhang, A. Otani and E.J. Maginn, J. Chem. Theory Comp. **11**, 3537 (2015).

[12] R. Hartkamp, P.J. Daivis and B.D. Todd, Phys. Rev. E **87**, 032155 (2013).

[13] J.G. Powles and D.M. Heyes, Mol. Phys. **98**, 917 (2000).

[14] K. Tankeshwar and K.N. Pathak, J. Phys.: Cond. Matt. **6**, 591 (1994).

[15] K. Tankeshwar and K.N. Pathak, J. Phys.: Cond. Matt.**7**, 5729 (1995).

[16] S. Singh, K. Tankeshwar, K.N. Pathak, and S. Ranganathan, J. Phys.: Cond. Matt. **18**, 1395 (2006).

[17] J.C. Dyre, Phys. Rev. E, **48** 400 (1993).

[18] J.W. Goodwin and R.W. Hughes, *Rheology for Chemists* (Roy. Soc. Chem., Cambridge, 2000).

[19] K. Tankeshwar, K.N. Pathak and S. Ranganathan, J. Phys.: Cond. Matt. **8**, 10847 (1996).

[20] I.S. Gradshteyn and I.M. Ryzhik, *Table of Integrals, Series and Products* (Academic Press, New York, 1980).

[21] T. Reytier, C. Bes, P. Marechal, M. Bianciardi and A. Santgerma, Int. Journ. Fatigue, **42**, 147 (2012).

[22] D. Levesque and L. Verlet, Mol. Phys. **61**, 143 (1987).

[23] K. Meier, A. Laesecke and S. Kabelac, J. Chem. Phys. **121**, 3671 (2004).

[24] L.V. Woodcock, AIChE Journal **52**, 438 (2006).

[25] D.J. Evans and G.P. Morriss, Phys. Rev. A **30**, 1528 (1984).

[26] A.J.C. Ladd, Mol. Phys. **53**, 459 (1984).

[27] W.P. Cox and E.H. Merz, J. Polym. Sci. **28**, 619 (1958).

[28] J.J. Erpenbeck, Phys. Rev. A **38**, 6255 (1988).

[29] A.J.C. Ladd, W.E. Alley and B.J. Alder, J. Stat. Phys. **48**, 1147 (1987).

[30] D.J. Evans Phys. Rev. A **23**, 1988 (1981).

[31] D.J. Evans, Physica A **118**, 51 (1983).

[32] R.F. Fox, Physica A **118**, 383 (1983).

[33] B.L. Holian and D.J. Evans, J. Chem. Phys. **78**, 5147 (1983).

[34] C. Trozzi and G. Ciccotti, Phys. Rev. A **29**, 916 (1984).

[35] J. C. Maxwell, Philos. Trans. R. Soc. London **157**, 49 (1867).

[36] P.G. Hoel, *Introduction to mathematical statistics*, 4th ed. (John Wiley & Sons, New York, 1971).

[37] G. E. P. Box and M.E. Muller, Annals Math. Stat. **29** 610 (1958).

[38] F.H. Stillinger and P.G. Debenedetti, J. Phys. Chem. B **109**, 6604 (2005).

[39] D. J. Evans, E.G.D. Cohen and G.P. Morriss, Phys. Rev. Lett. **71**, 2401 (1993).

[40] D. J. Evans and G.P. Morriss, Phys. Rev. A **38**, 4142 (1988).

[41] D. J. Evans and D. J. Searles, Adv. Phys. **51**, 1529 (2002).

[42] D. J. Searles and D. J. Evans, J. Chem. Phys. **112**, 972 (2000).

[43] M.S. Shell, P.C. Debeneditti and F.H. Stillinger, J. Phys.: Cond. Matt. **17**, S4035 (2005).

[44] S. Chowdhury, S. Abraham, T. Hudson and P. Harrowell, J. Chem. Phys. **144**, 124508 (2016).

[45] T. Keyes, G.V. Vijayadamodar and U. Zurcher, J. Chem. Phys. **106**, 4651 (1997).

[46] D. Antoniou and S.D. Schwartz, J. Chem. Phys. **115**, 4670 (2001).

[47] J.H.R. Clarke, JCS Faraday II **75**, 1371 (1979).

[48] J.H.R. Clarke, J.F. Maguire and L.V. Woodcock, Farad. Disc. **69**, 273 (1980).

[49] W. Kob, C. Donati, S.J. Plimpton, P.H. Poole and S.C. Glotzer, Phys. Rev. Lett. **79**, 2827 (1997).

[50] D. Zwillinger, *Standard Mathematical Tables and Formulae*, 30th Ed. (CRC Press, Boca Raton, 1996).

[51] T. Tsang and H. Tang, Phys. Rev. A, **15**, 1696 (1977).

[52] D.P. Dean and J.P. Kushik, J. Chem. Phys. **76**, 619 (1982).

[53] K. Koperwas, K. Adrjanowicz, Z. Wojnarowska, A. Jedrzejowska, J. Knapik and M. Paluch, Scientific Rep. **6**, 36934 (2016).

[54] E.R. Meyer, J.D. Kress, L.A. Collins and C. Ticknor, Phys. Rev. E **90**, 043101 (2014).

[55] D. Levesque and L. Verlet, Phys. Rev. A **2**, 2514 (1970).

[56] J. Kushick and B.J. Berne, J. Chem. Phys. **59**, 3732 (1973).

[57] S. Kambayashi and Y. Hiwatari, Phys. Rev. E **49**, 1251 (1994).

[58] P.A. Egelstaff and P. Schofield, Nucl. Sci. Eng. **12**, 260 (1962).

[59] J.P. Boon and S. Yip, *Molecular Hydrodynamics* (McGraw-Hill, New York, 1980).

[60] B.J. Alder and T.E. Wainwright, Phys. Rev. A **1**, 18 (1970).

[61] J.R.D. Copley and S.W. Lovesay, Rep. Progr. Phys. **38**, 461 (1975).

[62] J.J. Erpenbeck and W.W. Wood , Phys. Rev. A **43**, 4254 (1991).

[63] R. Zwanzig and M. Bixon, Phys. Rev. A, **2** 2005 (1970).

[64] P.E. Mason and T. Gaskell, Phys. Lett. A **80**, 395 (1980).

[65] D. Levesque and W.T. Ashurst, Phys. Rev. Lett. **33**, 277 (1974).

[66] A. McDonough, S.P. Russo and I.K. Snook, Phys. Rev. E **63**, 026109 (2001).

[67] T. Gaskell and S. Miller, J. Phys.: Solid State Matt. **11**, 4839 (1978).

[68] I.M. de Schepper, J.C. van Rijs, A.A. van Well, P. Verkerk, L.A. de Graaf and C. Bruin, Phys. Rev. A **29**, 1602 (1984).

[69] J.D. Gezelter, E. Rabani and B.J. Berne, J. Chem. Phys. **107**, 4618 (1997).

[70] H. Endo and Y. Endo, Progr. Theoret. Phys. **61**, 1569 (1979).

[71] D.C. Wallace, Phys. Rev. E **58**, 538 (1998).

[72] M. Vergeles and G. Szamel, J. Chem. Phys. **110**, 3009 (1999).

[73] A. Rahman, J. Chem. Phys. **45**, 2585 (1966).

[74] A. Rahman, Phys. Rev. A **136**, 405 (1964).

[75] H. Endo and Y. Endo, Prog. Theoret. Phys. **66**, 794 (1981).

[76] V. Yu Bardik, N.P. Malomuzh and K.S. Shakun, J. Chem. Phys. **136**, 244511 (2012).

[77] A. Verdaguer and J.A. Padró, Phys. Rev. E **62**, 532 (2000).

[78] Y. Endo and H. Endo, J. Chem. Phys. **80**, 2087 (1984).

[79] D. Thirumalai and R.D. Mountain, Phys. Rev. E **47**, 479 (1993).

[80] W. Kob and H.C. Andersen, Phys. Rev. E **51**, 4626 (1995).

[81] P. Hopkins, A. Fortini, A.J. Archerand M. Schmidt, J. Chem. Phys. **133**, 224505 (2010).

[82] C. De Michele and D. Leporini, Phys. Rev. E **63**, 036701 (2001).

[83] T. Odagaki and Y. Hiwatari, Phys. Rev. A **43**, 1103 (1991).

[84] S. Acharya, U.K. Nandi and A.M. Bhattacharyya, J. Chem. Phys. **146**, 134504 (2017).

[85] R.K. Sharma, K. Tankeshwar and K.N. Pathak, J. Phys.: Cond. Matt. **7**, 537 (1995).

Figure Captions

Figure 1: Upper Frame (a), Comparison between the normalized time correlation function, $C_s(t)$, from MD and its fitted forms, both gaussian (shifted upwards by 1) and sech. The brown curves are the fit to the gaussian expression given in Eq. (3), and the sech function of Eq. (4). The contributions of the three terms in each expression to the total fit are also shown on the figure. For the gaussian function, $A = 0.66135$, $B = 0.35820$, $\tau_1 = 0.0563258$, $\tau_2 = 0.261270$ and $\tau_3 = 0.260116$. and for the sech function, $A = 0.72637$, $B = 0.192605$, $\tau_1 = 0.0492775$, $\tau_2 = 0.182062$ and $\tau_3 = 0.572743$. The green filled in squares are the $c(t)$ values defined in Eq. (13) which was fitted to the MD viscuit data. The red squares are the difference between the MD and fitted correlation function. The Lennard-Jones (LJ) state point is $\rho = 0.8442$ and $T = 0.722$. The simulation data minus the least squares fit is shown as the red squares near the baseline. The lower frame (b) is as for frame (a) except the time dependent viscosity, $\eta_s(t)$ is plotted.

Figure 2: The real and imaginary parts of the frequency dependent viscosity, $\eta(\omega)$, directly from MD and from the gaussian and sech fit formulas. The real gaussian formula is given in Eq. (6) and the real sech expression is in Eq. (7). The imaginary gaussian formula is in Eq. (8) and the imaginary sech is in Eq. (9). The state point is $\rho = 0.8442$ and $T = 0.722$, and other details are as for Fig. 1. Finite shear rate viscosities are also plotted taken from NEMD data using the SLLOD method, where ω is replaced by $2\pi\dot{\gamma}$, and $\dot{\gamma}$ is the shear rate.[6]

Figure 3: Two dimensional conditional PDF of initial stress at time zero $\sigma(0)$ and at time t, $\sigma(t)$, for four times, $t = \{0.02, 0.05, 0.1, 2.5\}$. The contours shown are for the same stress values from the fit function given in Eq. (13). The value of $c(t)$ is shown in each frame. Frames (a)-(d) are in order of decreasing c. The range of shear stress is between -0.21 and 0.16 on

both axes. The 2D stress plots can be normalized by the standard deviation, in which case the range is, -2.96 to 2.25. The Lennard-Jones (LJ) state point, $\rho = 0.8442$ and $T = 0.722$ was used.

Figure 4: Viscuit analysis with in frame (a) the probability density function of the viscuits as defined in Eq. (15) after a time of 600 time steps (solid blue line). The red curve is the distribution of an autocorrelation of two independent gaussian number distributions, while the dashed black curve was generated from correlated gaussian numbers using Eqs. (4) for $c(t)$ and (14). In frame (b) the ratio, $R(\eta_u)$, defined in Eq. (17), is plotted on a lin-log scale. On the figure are given the following key numerical values, (i) the time t in units of number of time steps (each of 0.005), (ii) the corresponding time dependent viscosity, $\eta(t)$, and (iii) the A parameter defined in Eq. (17). The Lennard-Jones (LJ) state point was $\rho = 0.8442$ and $T = 0.722$.

Figure 5:(a) The $A(t)$ parameter, where t is the duration of the viscuit, in the exponential given in Eq. (17), and a least squares fit curve going through the data points.

Figure 5:(b) A 2D probability distribution map of the trace of the time dependent viscuits taken up to 600 time steps on the abscissa against the initial time origin shear stresses. The accumulated probability density function of these traces was obtained from over 15 million starting trajectories and is shown in the background. Some individual viscuit trajectories are also shown superimposed on the map (Multimedia view).

Figure 6: Upper Frame (a): The PDF of the initial shear stress σ_0 (blue symbols) and that of the visclet (red symbols) with $M = 120$. They are represented very well by, respectively, a gaussian with the analytic form for $P(\sigma_0)$ given in Eq. (11) and $x^2P(x)$, see Eq. (18), respec-

tively, fitted to the MD data. The $*$ symbols are the initial stress dependent relaxation times or $\tau_{s,0}$. Lower Frame (b) As for frame (a) except on a lin-log scale.

Figure 7: The $C_{s,0}(t)$ defined in Eq. (19) for four bands of initial stress, σ_0. Key: $\sigma_0/S(\sigma_0)$ in the range $0-1$, $1-2$, $2-3$ and $3-4$, which are also indicated on the figure. The state points are from bottom to top T, ρ: (a) 0.722, 0.8442, (b) 0.500, 0.8442, and (c) 0.500, 0.9211. The latter two states are in the metastable liquid region of the phase diagram. The pressures are close to zero for (a) (0.148) and (c) (-0.025) but slightly negative for (b) (-1.363). The green curves are the GK total stress relaxation and the lower magenta curves are fits for $t > 0.4$ to the exponential form, $C_s(t) = A\exp(-Bt)$, where A, B are for the curve sets from bottom to top are: $0.146, 2.31$, $0.184, 1.45$ and $0.200, 0.569$ for the three state points, respectively.

Figure 8: Upper Frame (a): The VACF and least squares fit using Eq. (25) fit for the state point $\rho = 0.8442$ and $T = 0.722$, with $N = 4000$. Key: The constants for Eq. (25) are: $\tau_1 = 0.1071$, $\tau_2 = 0.2250$, $\tau_3 = 0.1240$, $\tau_4 = 0.09222$, $A = 18.50$, $B = -88.85$, and $C = 1217.7$. The lower frame (b): The time dependent diffusion coefficient, $D(t)$ directly from the MD simulation and from the integral of the fitted VACF of Eq. (25) leading to Eq. (26).

Figure 9: The mean square displacements, $\Delta r^2(t)$ calculated directly and from the velocity autocorrelation function using Eq. (23). The upper brown line is the long time limiting formula $A + 6Dt$. The difference between $A + 6Dt$ and the actual MSD is the red curve, and the fit to this using the expression in Eq. (28) is the black line. The constants are $A = 0.021813$, $B = 0.025424$, $\tau_1 = 0.134862$, $D = 0.033234$ and $\delta t = -0.05$. The magenta curve is the short time ballistic region of the analytic form, $\Delta r^2(t) = 3k_BTt^2/m$. The state point is $\rho = 0.8442$ and $T = 0.722$.

Figure 10: Upper Frame (a): The real part of the cosine Fourier transform of the VACF $D'(\omega)$. The 4 components and total 'T' from Eq. (30) are shown as solid lines. The corresponding numerical integration of the four components of the analytic VACF defined in Eq. (25) are also shown as symbols. The lower Frame (b) is as for the upper frame, except the sine or imaginary part of the Fourier transform of the VACF, *i.e.*, $D''(\omega)$ from Eq. (31), is plotted.

Figure 11: $D'(\omega)$ and $D^*(\omega)$ obtained directly from the MD simulation data by numerical integration. A power law decay, denoted on the figure by 'P.L.' of the form, A_p/ω^p, where $A_p = 1.57 \times 10^6$ and $p = 5.564$ are least square fits to the data in the range, $55 > \omega > 35$. The formula,[76] $D' = Aa(\tau_a\omega)^q \exp(-(\tau_a\omega)^q)$ where $\tau_a = 0.822$, $p = 0.632$ and $q = -0.0752$ from the given formulas and $Aa = 21.50$ by fitting to the simulation data in the frequency range, $55 > \omega > 30$ which is denoted by 'P.E.' on the figure. 'Fit anal.' and 'Fit num.' are numerical transforms of the fitted $C_v(t)$ shown in Eq. (25). Note the log-log scale. The state point is $\rho = 0.8442$, and $T = 0.722$.

Figure 12: The $C_{v,i}(t)$ defined in Eq. (34) for four bands of initial velocity, v_0. Key: v_0/σ_v in the range $0-1$, $1-2$, $2-3$ and $3-4$, which are also indicated on the figure. The state point is $\rho = 0.8442$, and $T = 0.5$ and $T = 0.722$.

Figure 13: In the upper frame (a) is shown, $W(r,t)$, defined in Eq. (36) for three times (given on the figure) computed directly in the MD simulations. The analytic solution of the self van Hove function in Eq. (35) using Eq. (28) for the mean square displacement is also shown as a continuous red curve. The lower frame (b) gives the non-gaussian function, $\alpha(t)$ and the mean square displacement.

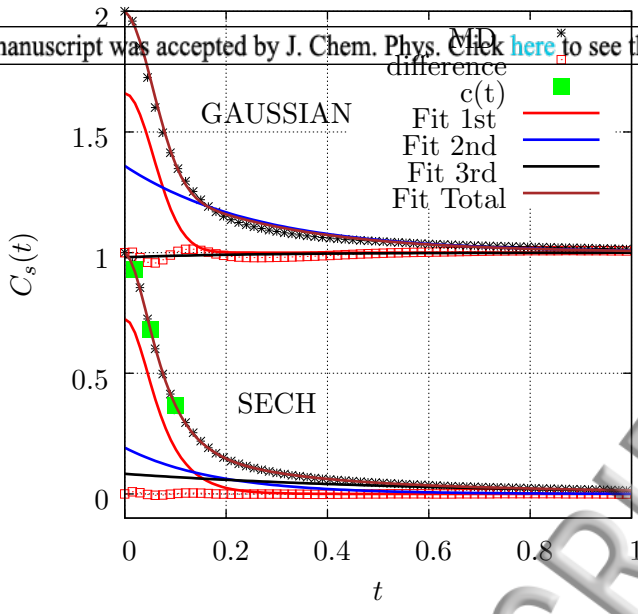

(a)

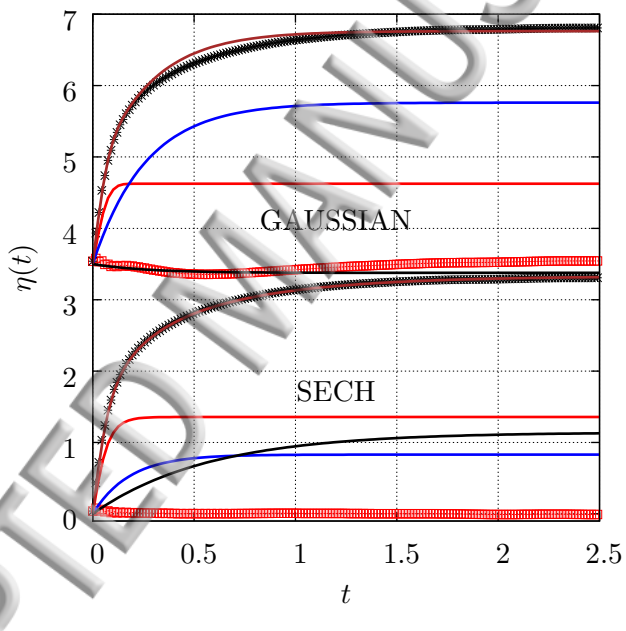

(b)

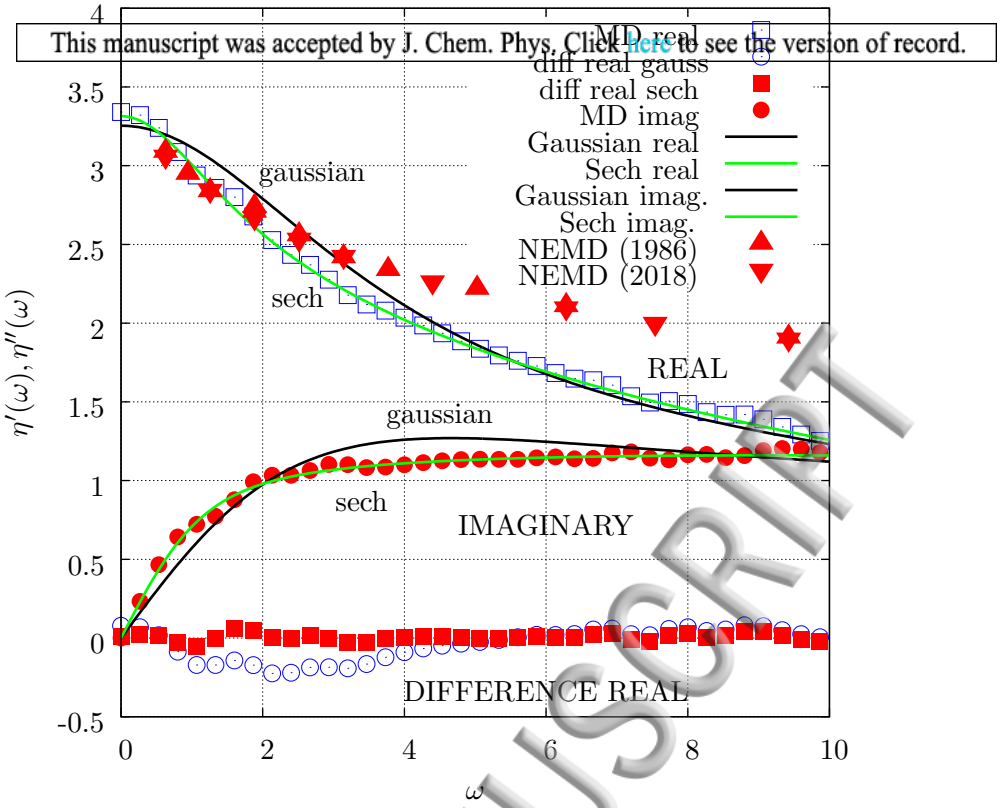

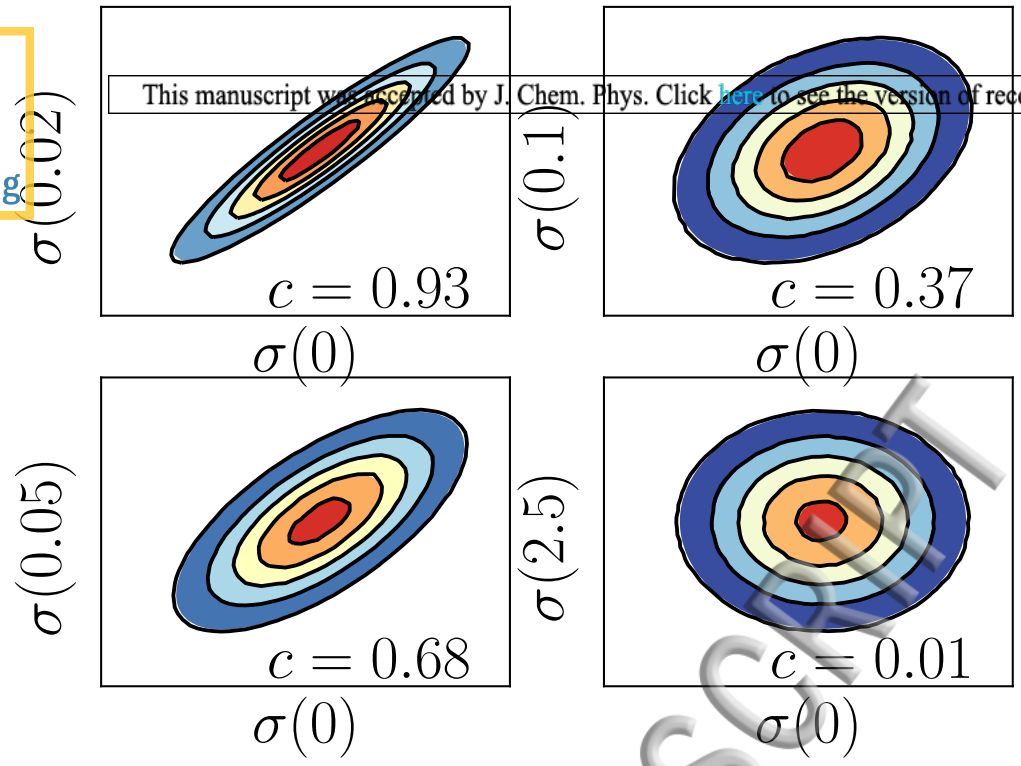

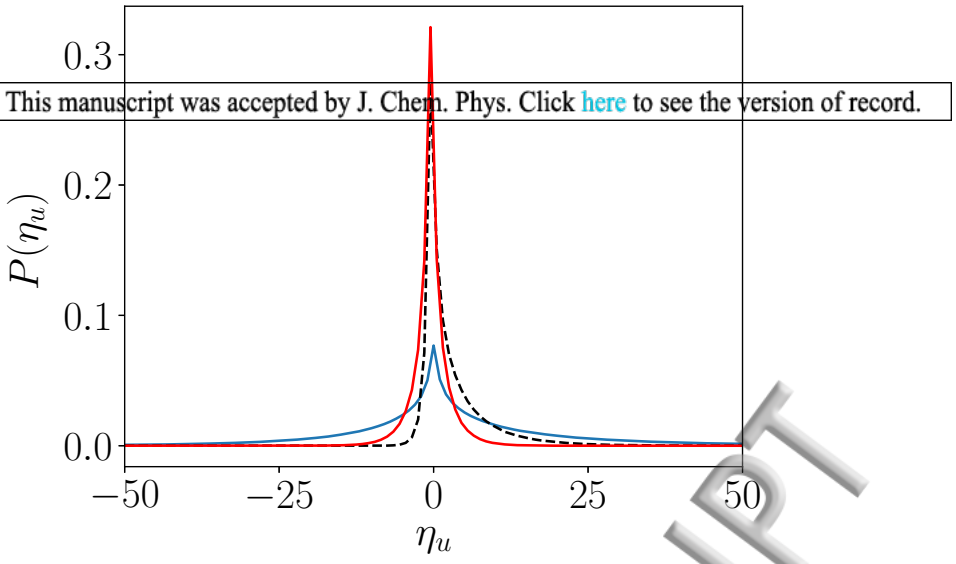

(a)

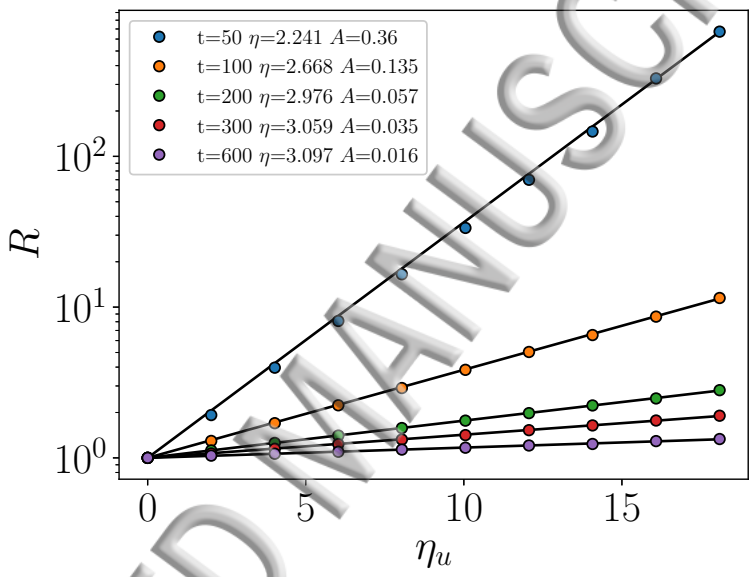

(b)

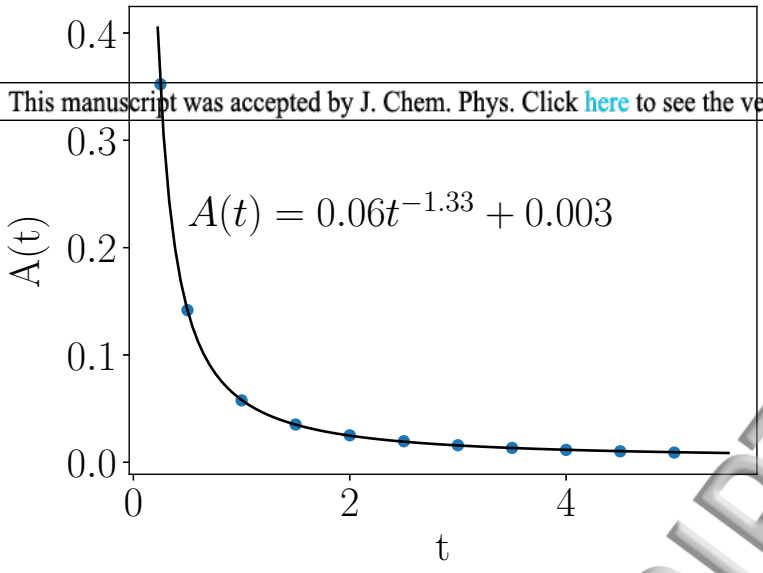

(a)

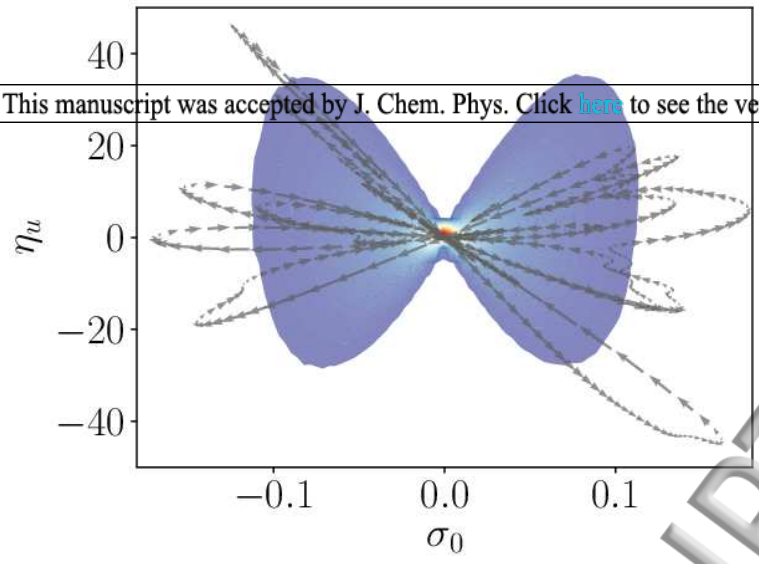

(b)

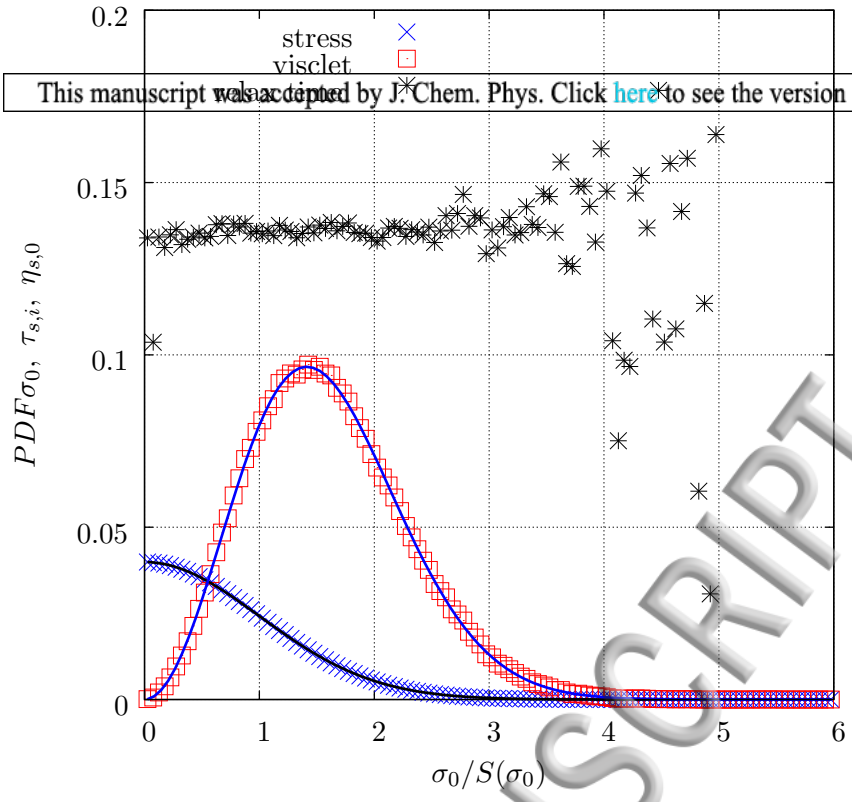

(a)

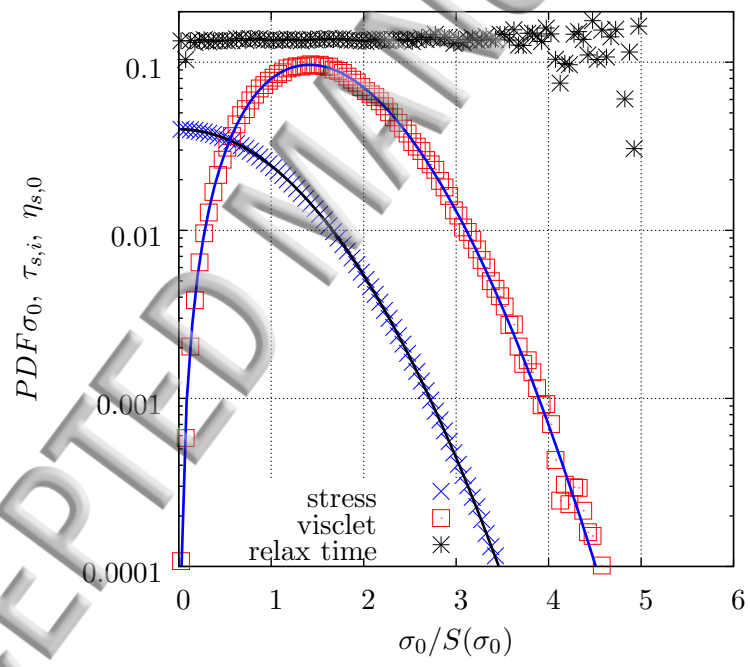

(b)

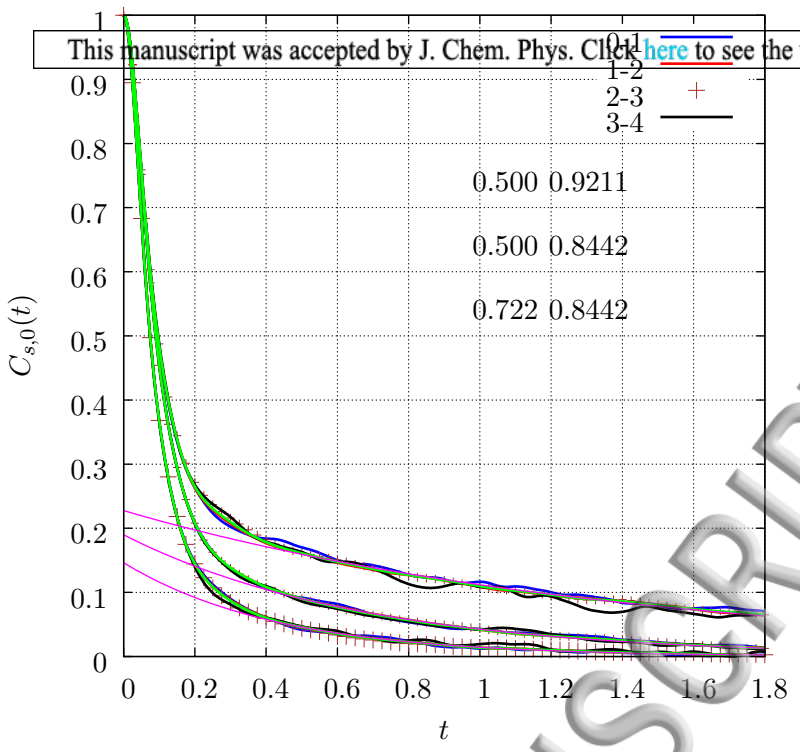

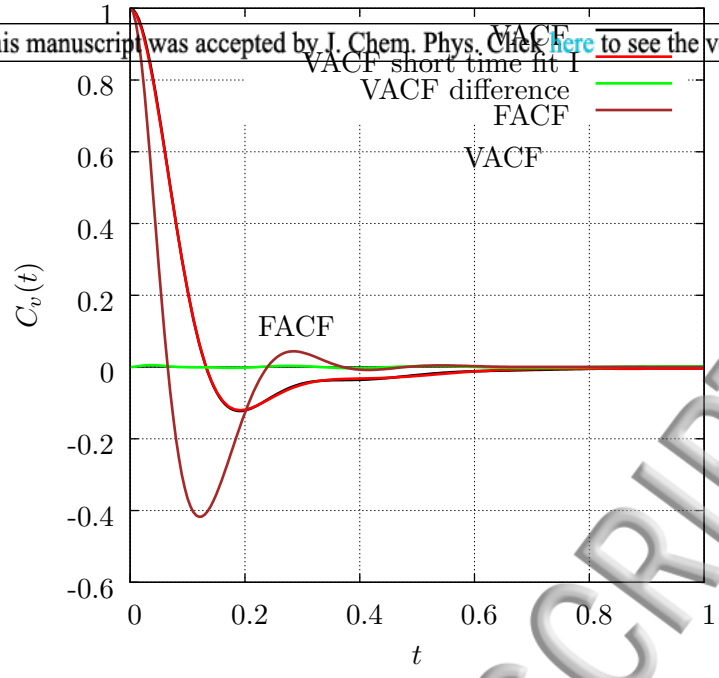

(a)

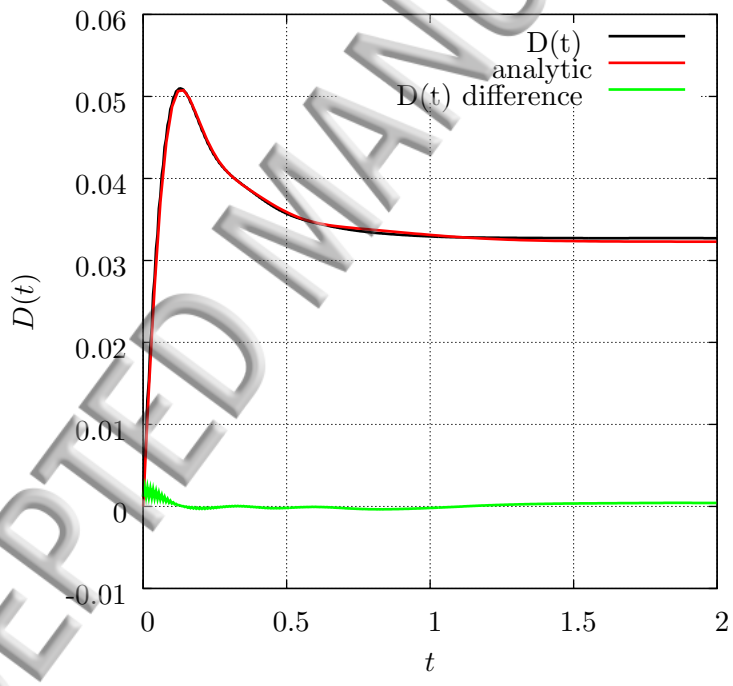

(b)

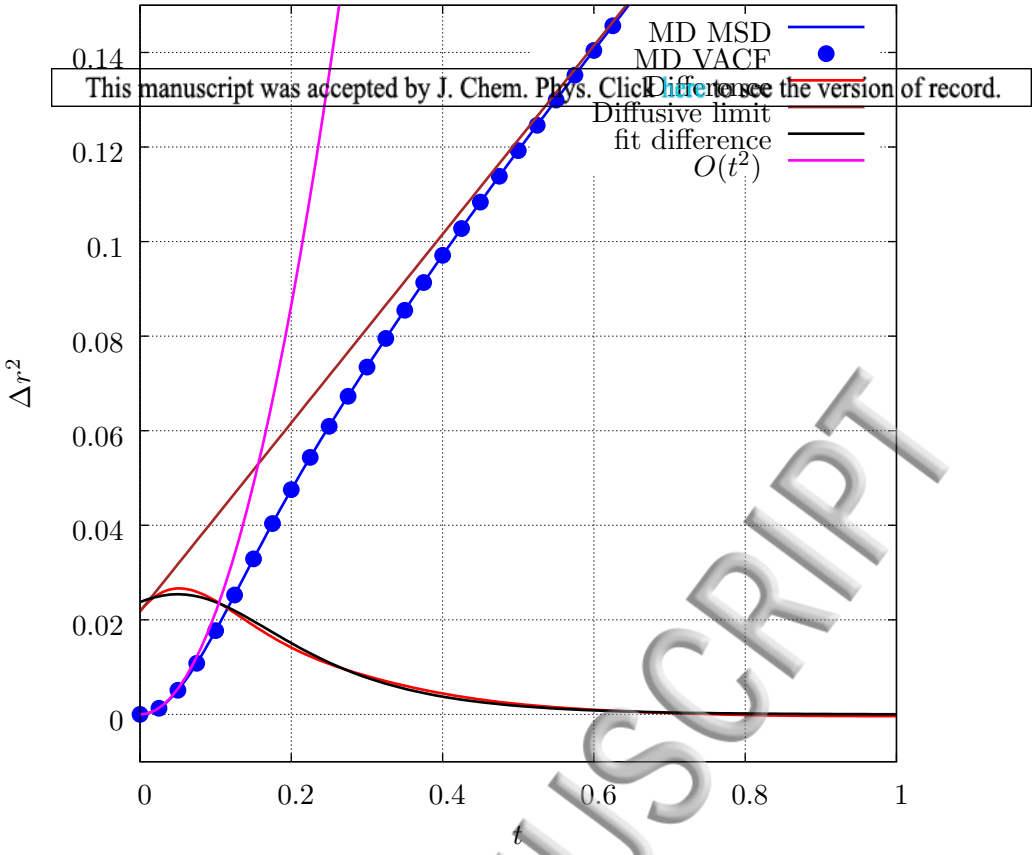

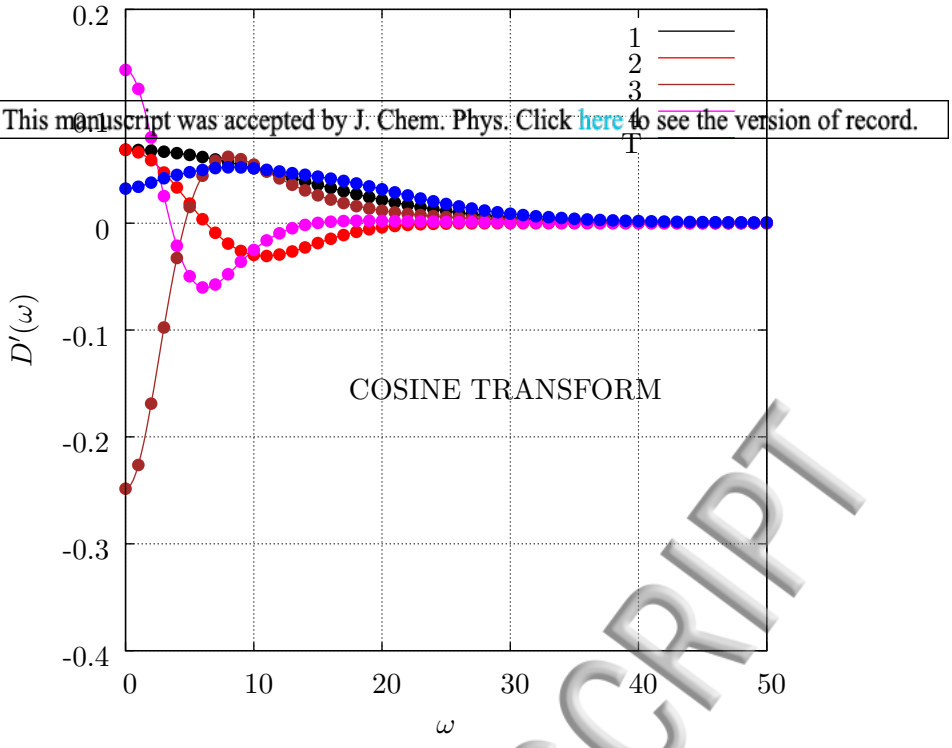

(a)

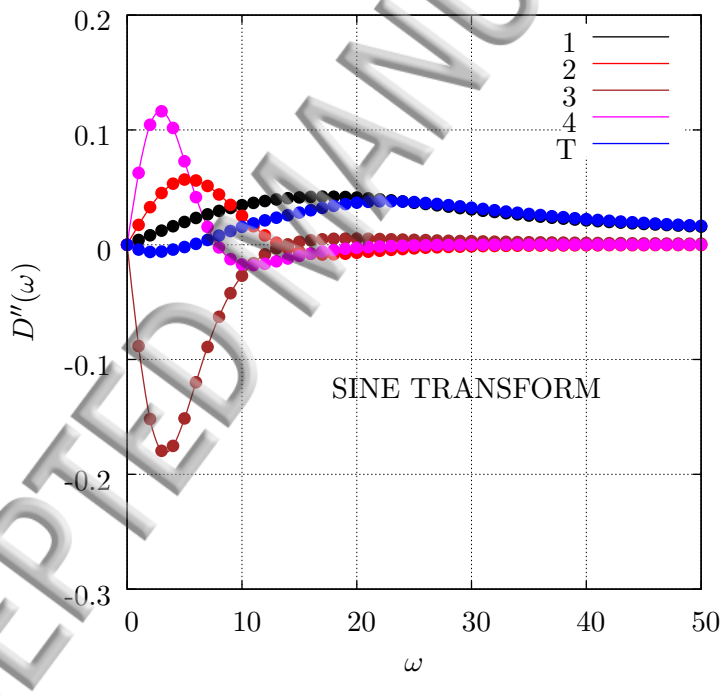

(b)

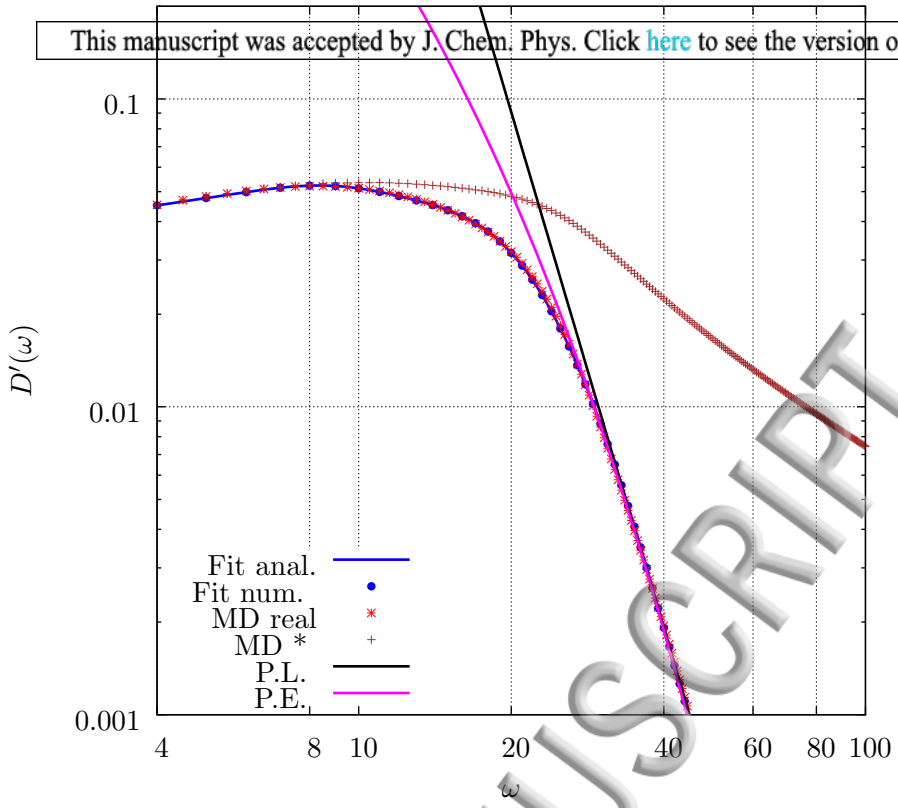

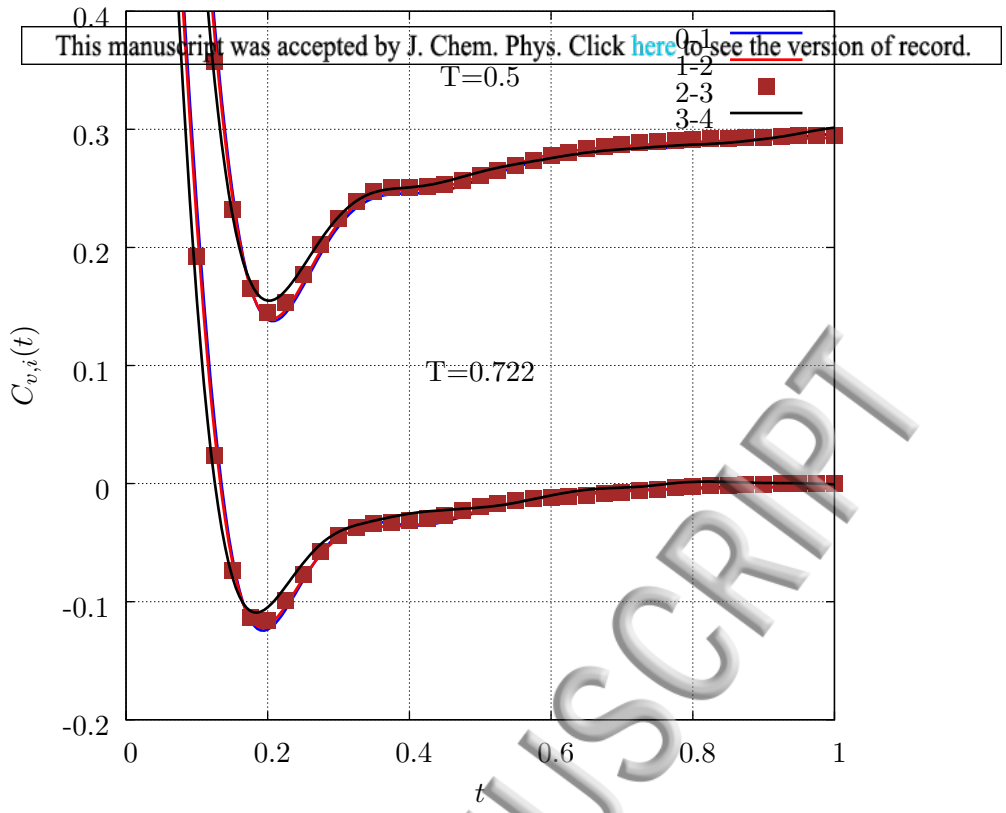

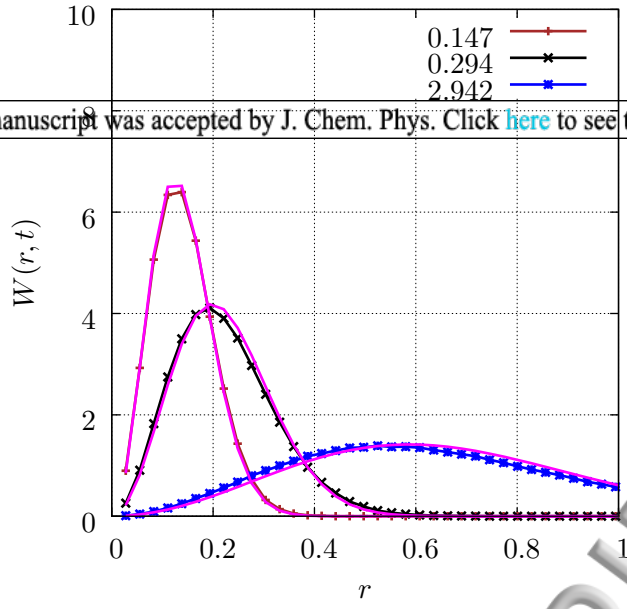

(a)

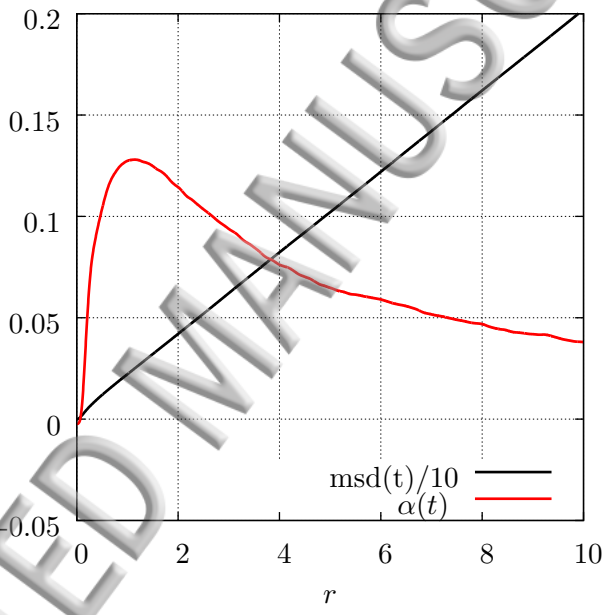

(b)